J. Fluid Mech. (1990), *vol.* 211, *pp.* 1–35
Printed in Great Britain

Theoretical study of turbulent channel flow: bulk properties, pressure fluctuations, and propagation of electromagnetic waves

By V. M. CANUTO[1], G. J. HARTKE[1], A. BATTAGLIA[1], J. CHASNOV[1] AND G. F. ALBRECHT[2]

[1] NASA Goddard Space Flight Center, Institute for Space Studies, 2880 Broadway, New York, NY 10025, USA

[2] Mail Code L, Lawrence Livermore National Laboratory, Livermore, CA 94550, USA

(Received 6 October 1988 and in revised form 29 June 1989)

In this paper, we apply two theoretical turbulence models, DIA and the recent GISS model, to study properties of a turbulent channel flow. Both models provide a turbulent kinetic energy spectral function $E(k)$ as the solution of a nonlinear equation; the two models employ the same source function but different closures. The source function is characterized by a rate $n_s(k)$ which is derived from the complex eigenvalues of the Orr–Sommerfeld equation in which the basic flow is taken to be of a Poiseuille type. The Orr–Sommerfeld equation is solved for a variety of Reynolds numbers corresponding to available experimental data. A physical argument is presented whereby the central line velocity characterizing the basic flow, U_0^L, is not to be identified with the U_0 appearing in the experimental Reynolds number. A renormalization is suggested which has the effect of yielding growth rates of magnitude comparable with those calculated by Orszag & Patera based on their study of a secondary instability. From the practical point of view, this renormalization frees us from having to solve the rather time-consuming equations describing the secondary instability. This point is discussed further in §13. In the present treatment, the shear plays only the role of a source of energy to feed the turbulence and not the possible additional role of an interaction between the shear of the mean flow and the eddy vorticity that would give rise to resonance effects when the shear is equal to or larger than the eddy vorticities. The inclusion of this possible resonance phenomenon, which is not expected to affect the large-eddy behaviour and thus the bulk properties, is left for a future study. The theoretical results are compared with two types of experimental data: (*a*) turbulence bulk properties, table 4, and (*b*) properties that depend strongly on the structure of the turbulence spectrum at low wavenumbers (i.e. large eddies), tables 5 and 6. The latter data are taken from recent experiments measuring the changes in the propagation of an electromagnetic wave through a turbulent channel flow. The fluctuations in the refractive index of the turbulent medium are thought to be due to pressure fluctuations whose spectral function $\Pi(\boldsymbol{k})$ is contributed mostly by the interaction between the mean flow and the turbulent velocity. The spectrum $\Pi(\boldsymbol{k})$ must be computed as a function of the wavenumber $\boldsymbol{k}$, the position in the channel x_2, and the width of the channel Δ. The only existing analytical expression for $\Pi(\boldsymbol{k})$, due to Kraichnan, cannot be used in the present case because it applies to the case $x_2 = 0$ and $\Delta = \infty$, which corresponds to the case of a flat plate, not a finite channel. A general expression for $\Pi(\boldsymbol{k}, x_2; \Delta)$ is derived here for the first time and employed to calculate the fraction of incoherent radiation scattered out of a coherent beam. In

§11, we treat anisotropy and show how to extend the previous results to include an arbitrary degree of anisotropy α in the sizes of the eddies. We show that the theoretical one-dimensional spectra yield a better fit to the data for a degree of anisotropy ($\alpha \approx 4$) that is within the range of experimental values. We also extend the expression for $\Pi(\boldsymbol{k}, x_2; \Delta)$ to $\Pi(\boldsymbol{k}, x_2; \Delta, \alpha)$ and compute the pressure fluctuations for different values of α. Similarly, we evaluate the fraction of electromagnetic energy scattered by an anisotropic turbulent flow and find a good fit to the laboratory data for a value of $\alpha \approx 4$–6. Scaling formulae for the scattered fraction are presented in §12. These formulae reproduce the calculated results, both with and without the addition of anisotropy, to better than 5%.

Theoretical problems however remain which will require further study: among them, lack of backscatter (i.e. the transfer of energy from large to small wavenumbers) in the GISS model, possible resonance effects between the shear and eddy vorticity, behaviour of the one-dimensional spectral function at low wavenumbers, and the role of the secondary instability. These topics are now under investigation.

---

1. Introduction

Experimental data on turbulent channel flow (see Laufer 1951; Comte-Bellot 1963; Clark 1968; Hussain & Reynolds 1975; Willmarth 1975; Johansson & Alfredsson 1982) can be used to test the validity of theoretical descriptions of turbulence. The latter can be broadly divided into two categories: numerical simulation of the Navier–Stokes equations and theoretical closure models.

While direct numerical simulations (Kim, Moin & Moser 1987; Moin & Kim 1982) have successfully reproduced several experimental data, they are limited to low Reynolds numbers since the number of grid points required increases according to the $\frac{9}{4}$ power of the Reynolds number and the number of time steps needed for an accurate simulation increases according to the $\frac{3}{4}$ power, yielding a rate of increase of Reynolds number to the third power. For high-Reynolds-number flows, the required number of grid points rapidly outstrips presently available computational facilities. To treat high-Reynolds-number turbulent flows, large-eddy simulations make use of (empirical) subgrid-scale models (Moin & Kim 1982).

Theoretical closure models can be broadly divided into two categories: single-point and two-point closure models. The most well known among the former is the one originally proposed by Hanjalic & Launder (1972) (HL), which proved successful in describing several types of shear flows. The HL model provides three coupled differential equations for the Reynolds stress tensor τ_{12}, the energy dissipation rate ϵ, and the turbulent kinetic energy K, defined as the integral over all wavenumbers k of the turbulent energy spectral function $E(k)$. While the HL model has proven very successful in the detailed description of several types of shear flows, its main drawback is the presence of six free parameters that the model cannot determine.

In the early seventies, Leslie (1973) was the first to consider in detail the possible application of two-point closure models to turbulent channel flow. Upon realizing the unmanageable complexity of the DIA equations for the general case of shear flow (see Kraichnan 1964*b*), Leslie tried to develop a systematic programme of simplifications for the two-point closure equations by restricting the analysis to the case of anisotropic but homogeneous flow (i.e. with constant shear) in the hope of deriving in a deductive, parameter-free fashion, the empirical one-point closure relations of

Hanjalic & Launder (1972). By his own admission, Leslie did not succeed in his attempt.

Since Leslie's work was not followed by other systematic attempts to apply two-point closure models to turbulent channel flow (see however Tchen 1953 and Hinze 1975), one is left today with: (*a*) the successful one-point HL closure model which, however, contains six free parameters to be determined from experiments, (*b*) direct numerical simulations with their intrinsic Reynolds-number limitations, and (*c*) large-eddy simulation which must rely on the use of a subgrid-scale model.

The lesson learned from Leslie's work is that a full treatment of the anisotropy is just not possible at present. It may also mean that to make progress one must begin with exactly the opposite point of view, namely with the simplest treatment, so as to be able to incorporate progressively more complex models of anisotropy. To be specific, in this paper we shall adopt the following approach: first, we employ two models of turbulence: the growth instability spectral solution (GISS) model and the direct interaction approximation (DIA) that differ in the degree of complexity with which they treat the nonlinear transfer terms. Both models have already been validated in the case of isotropic turbulence (Canuto, Goldman & Chasnov 1987) where they were shown to yield similar bulk properties. The GISS model is much simpler to use than DIA which requires rather extensive numerical labour, although it cannot claim the *a priori* validation that makes DIA an attractive theory. Since the quantities calculated with these two models refer to isotropic cases, whereas in the case of channel turbulence the mean flow is known to stretch the eddies in the streamwise direction, the expressions for the quantities of interest (e.g. the one-dimensional energy spectrum, the amplitude of the pressure fluctuations, and the attenuation of a laser beam) must be expressed in the physical, anisotropic system where the wavenumbers are denoted by $\boldsymbol{k}'$, with $k'_x \neq k'_y$, and where the basic function is the turbulent energy spectral function, $E(\boldsymbol{k}')$. The transformation from the $\boldsymbol{k}$ to the $\boldsymbol{k}'$ system is done via the introduction of an anisotropy function, $\alpha(\boldsymbol{k}')$, a measure of the stretching of the eddies in the streamwise direction, such that $k'_x = k_x/\alpha$, $k'_y = k_y$, and $k'_z = k_z$. In this paper, we have investigated two functional forms for $\alpha(\boldsymbol{k}')$.

(i) α = constant

We show that with $5 \leqslant \alpha \leqslant 8$, we obtain a considerable improvement with respect to the isotropic case (for which $\alpha = 1$) for three experimentally measured sets of data on: (*a*) one-dimensional turbulent spectra at different Reynolds numbers, figure 12, (*b*) pressure fluctuations at the wall of a turbulent channel flow, figures 14 and 15, and (*c*) propagation of electromagnetic waves in turbulent channel flow, figure 16. We may further notice that the value for the pressure fluctuations so obtained is very close to that derived using full numerical simulations of the Navier–Stokes equations, which have also indicated that the degree of stretching for the largest eddies is approximately that given by the above value of α.

The assumption of constant α implies that all the eddies, irrespectively of their sizes, are stretched by exactly the same amount by the mean flow. This assumption clearly cannot hold for the inertial eddies that are usually isotropic, having originated from multiple break-ups of the larger eddies and having therefore undergone a great deal of isotropization. For this reason, we have investigated a second function for α.

(ii) $\alpha = \alpha(k)$

The function chosen (see (89) and the accompanying text) is constant for small wavenumber and monotonically decreases to unity with increasing wavenumber. This is the simplest functional form that embodies the correct physics. It was found that the use of this function with $\alpha = 5$ at small wavenumbers results in a better fit to the one-dimensional energy spectra than with constant α.

Concerning notation, while in the DIA the energy spectral function is denoted by $E(k)$, in the GISS model use is made of the function $F(k) = 2E(k)$.

2. The GISS model

Since the model has been described in detail in Canuto *et al.* (1987), we shall quote here only the basic equations. If $\epsilon(k)$ is the energy input from the external source into the interval $[0, k]$, the turbulent energy spectral function $E(k)$ is found as a solution of the following equations:

$$\epsilon(k) = 2\nu \int_0^k k^2 E(k)\,\mathrm{d}k + \int_k^\infty T(k)\,\mathrm{d}k, \tag{1}$$

where $\epsilon(k)$ is defined as

$$\epsilon(k) = 2\int_0^k (n_s(k) + \nu k^2)\, E(k)\,\mathrm{d}k. \tag{2}$$

The right-hand side of (1) tells us that the energy input $\epsilon(k)$ is partly dissipated by molecular viscosity, ν, and partly transferred by the nonlinear term, $T(k)$. The DIA and the GISS models differ in the way they describe the transfer function $T(k)$. In both models, however, one must prescribe the function $n_s(k)$ which represents the rate at which energy is being fed into the system. A discussion of how to compute this quantity will be given in §4. For the time being, we shall only note that the structure of $n_s(k)$ must be such that it depends on the source of energy for the turbulent flow, namely the shear itself. That this is indeed the case will be shown in (24) and (25). As for the transfer term $T(k)$, it is taken to be the product of a turbulent viscosity $\nu_t(k)$, times a mean-square vorticity $y(k)$, i.e.

$$\int_k^\infty T(k)\,\mathrm{d}k = \nu_t(k)\, y(k), \quad y(k) = \int_0^k k^2 F(k)\,\mathrm{d}k, \tag{3}$$

where

$$\nu_t(k) = \int_k^\infty \frac{F(k)}{n_c(k)}\,\mathrm{d}k. \tag{4}$$

Here $n_c(k)$ is a correlation time between eddies, to be determined by a closure. As shown in Canuto *et al.* (1987), the GISS model closure can be expressed as

$$2\gamma n_c(k) = n_s(k) + [n_s^2(k) + 4\gamma y(k)]^{\frac{1}{2}}, \tag{5}$$

which represents a balance between the source timescale n_s^{-1} and the inertial timescale $y^{-\frac{1}{2}}$. We may note that when $\epsilon(k) \to \epsilon =$ constant and $n_c \approx y^{\frac{1}{2}}$, (1) admits the well-known Heisenberg–Kolmogorov inertial spectrum $E(k) \propto k^{-\frac{5}{3}}$. As discussed in Canuto *et al.* (1987), the GISS model closure, (5), is able to reproduce both the inertial subrange as well as the low-wavenumber region which contains most of the energy, which dominate the bulk properties of interest here.

Once a source function, n_s, is chosen, (1)–(5) yield the energy spectral function $E(k)$. The GISS model contains only one parameter γ, see (5), which is fixed once and

for all since it is related to the Kolmogorov constant Ko by the expression (Canuto *et al.* 1987)

$$\gamma = \left(\frac{2}{3Ko}\right)^3. \tag{6}$$

The value adopted here for the Kolmogorov constant is $Ko = 1.65$.

As discussed in Canuto *et al.* 1987, the GISS model has been applied to a variety of cases with results satisfactory not only with respect to the available data but also with respect to the results of other models like DIA, the renormalization group (RNG) method, etc. (For details, see table VII of Canuto *et al.* 1987.)

3. The DIA model

Perhaps the most well known of the presently available theories to describe fully developed turbulence is Kraichnan's (1964*a*) direct interaction approximation (DIA) which in turn has given rise to other theories in the same spirit. We shall not discuss here the eddy-damped quasi-normal Markovian (EDQNM) approximation, which is phenomenological in nature, since the eddy correlation timescale (which within the DIA is determined by solving the integral equation satisfied by the infinitesimal response function) must be chosen using external inputs. A very complete description of EDQNM, its successes and limitations in describing 'universal' properties, can be found in Lesieur (1987).

Since the DIA has been described in detail in Leslie (1973), we shall present only the basic equations for the turbulent energy spectral function. The DIA is a well-understood approximation to the nonlinear transfer terms (see Martin, Siggia & Rose (1973) and it can be regarded as a fully deterministic theory without free parameters. Since the DIA formalism has in the past been applied primarily to describe those properties of turbulence that do not depend on the specific nature of the source function, experimental data concerning bulk properties could not be dealt with. To include them, the DIA was recently applied with good results to a set of model equations with a source function appropriate to high-Rayleigh-number convection. Perhaps the main drawback in the application of the DIA formalism to specific cases of interest has been the rather intimidating nature of the equations describing the turbulent energy spectral function, $E(k)$. Moreover, with the presence of the infinitesimal response function $G(k)$, one must in fact solve two coupled integral equations for $E(k)$ and $G(k)$. These equations may be written (Hartke, Canuto & Dannevik 1988)

$$\left(\frac{\partial}{\partial t} - n_s(k)\right) Q(k, t-s)$$
$$= 2\pi \iint^{\Delta} kqpb(k,q,p)\,\mathrm{d}q\,\mathrm{d}p \left(\int_{-\infty}^{s} \mathrm{d}s' G(k, s-s')\, Q(q, t-s')\, Q(p, t-s') - \int_{-\infty}^{t} \mathrm{d}s' G(q, t-s')\, Q(p, t-s')\, Q(k, s-s') \right) \tag{7}$$

and

$$\left(\frac{\partial}{\partial t} - n_s(k)\right) G(k, t-s)$$
$$= -2\pi \iint^{\Delta} kqpb(k,q,p)\,\mathrm{d}q\,\mathrm{d}p \int_{s}^{t} \mathrm{d}s' G(q, t-s')\, Q(p, t-s')\, G(k, s-s') + \delta(t-s), \tag{8}$$

where $Q(k,t-s) = \frac{1}{2}\langle u_i(\boldsymbol{k},t)\, u_i(-\boldsymbol{k},s)\rangle$, $\boldsymbol{u}(\boldsymbol{k},t)$ is the spatial Fourier transform of the turbulent velocity, the angular brackets denote a realization average, t and s are time variables, the energy spectrum is given by $E(k) = 4\pi k^2 Q(k,0)$, $b(k,q,p) = (q/k)\,(xy+z^3)$ with x, y, and z the cosines of the angles opposite $\boldsymbol{k}$, $\boldsymbol{q}$, and $\boldsymbol{p}$, respectively, $\delta(x)$ is the Dirac delta function, and the Δ over the wavenumber integrals indicates that the region of integration is restricted to a subdomain in which $\boldsymbol{k}$, $\boldsymbol{q}$, and $\boldsymbol{p}$ form a triangle. Once the growth rate $n_s(k)$ is specified, (7) and (8) can be solved for the energy spectrum and the infinitesimal response function.

The well-known drawback of the DIA, i.e. the prediction of a $-\frac{3}{2}$ rather than $-\frac{5}{3}$ inertial range, has little effect on the bulk properties of interest here since the inertial region is energy-poor compared with the low-wavenumber region.

4. The rate $n_s(k)$

Neither the DIA nor the GISS model can be expected to fix the functional form of $n_s(k)$ which must be provided by considerations other than the ones that led to the equations for the kinetic energy spectral function $E(k)$. Because of (2), prescribing $n_s(k)$ is physically equivalent to prescribing an equation for the energy rate $\epsilon(k)$. Our model can thus be considered a two-equation model, one for the kinetic energy $E(k)$ and the second equation for $\epsilon(k)$ which must be described from outside the problem via the rate $n_s(k)$.

Since n_s characterizes a fully turbulent regime, long after the transition from the laminar state has occurred, it cannot *a priori* be identified with the instability function n_s^{L-T} that characterizes the transition between laminarity (L) and turbulence (T), even though the processes they represent are physically equivalent. To derive n_s^{L-T}, one has a well-defined mathametical formalism, the stability theory. To derive $n_s(k)$ or, equivalently, $\epsilon(k)$, one would have to construct another equation thus making the model much more complex. We have already shown (Canuto *et al.* 1987) that physical arguments can be very helpful. Some general considerations are in order. First, it is known experimentally that, for example, in thermal convection the large-scale structures that one observes at the transition do persist in the turbulent phase, i.e. their structure survives the strongly diffusive and shearing action of a turbulent flow. This result is perhaps not unexpected since the large-scale structures have the longest lifetimes of all the eddies and also because their structure is affected primarily by the source rather than by the nonlinear transfer interactions. Stated differently, since the largest eddies cannot originate from even larger ones, their sole source of growth is the source itself. Second, from a mathematical point of view it would clearly be greatly advantageous if one could employ, even if partially, the well-established mathematical framework of stability theory to gain information about the form of the function $n_s(k)$. Here we want to make a clear distinction between the shape of the function $n_s(k)$ and its amplitude. We shall propose, and try to justify, that the former can be arrived at by the use of the Orr–Sommerfeld equation, while the latter can be arrived at only by providing a way to account for the presence of a turbulent flow. The latter is in fact likely to renormalize in a significant way the amplitudes of the parameters characterizing the laminar regime. This in turn translates into a renormalization of the Orr–Sommerfeld equation itself. The success of the calculations presented in this paper will be seen to depend to a large extent on the proper implementation of this renormalization procedure. Since the latter depends on the specific problem at hand, it cannot be formulated in a universal fashion. Each physical problem brings in its own characteristic features.

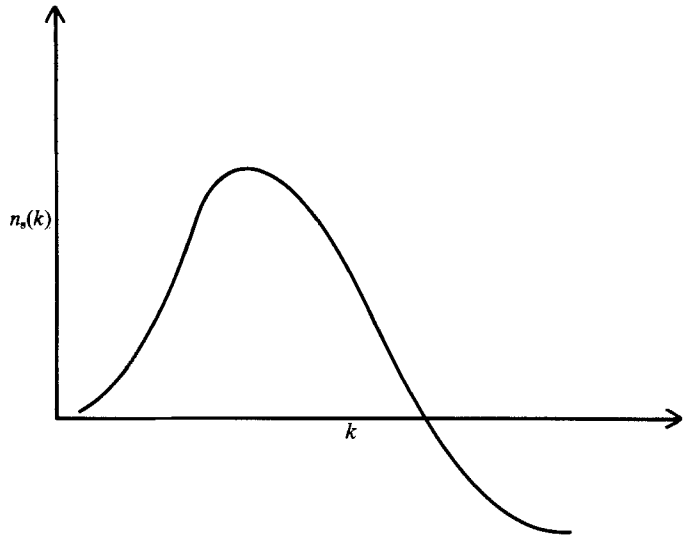

FIGURE 1. The expected general shape of the growth rate $n_s(k)$ *vs.* k. At large wavenumbers, $n_s(k)$ tends to $-\nu k^2$.

From the point of view of trying to understand a complex phenomenon like turbulence, we consider this to be an advantage, for the method requires an understanding of the renormalization that the most prominent features of the laminar flow have undergone. The use of an Orr–Sommerfeld type of equation to determine the functional form of the rate n_s is proposed here because such a function has features of almost universal character that are bound to be sufficiently well described by such an approach. First, consider the shape of $n_s(k)$. For wavenumbers less than $k_0 = 1/L$, where L is the geometrical dimension of the system under consideration, there cannot be any forcing and so n_s must be less than or equal to zero. On the other hand, for large values of k, i.e. when one deals with small eddies, the dominant mechanism is kinematic viscosity which contributes a factor $-\nu k^2$, i.e. the function n_s must become negative at some large value of k. In Canuto *et al.* 1987 it was shown that the GISS model requires that for large $k, n_s \sim -\nu k^2$ quite independently of its behaviour at low wavenumber, i.e. of the specific mechanism that feeds energy into the turbulent regime. One may therefore conclude that the general shape of this function must be of the form shown in figure 1. In our experience with different types of turbulence, i.e. grid turbulence, thermal convection, and shear, we have indeed verified that the physical $n_s(k)$ has the form of figure 1. For example, in the case of grid turbulence where both the kinetic energy spectral function $E(k)$ and the nonlinear transfer term $T(k)$ have been measured experimentally, one can derive $n_s(k)$ directly from the data since from (1) and (2) it follows that

$$2n_s(k) = -\frac{T(k)}{E(k)}. \tag{9}$$

The functions $E(k)$ and $T(k)$ are presented in figures 14 and 16 of Canuto *et al.* 1987. As one can see, the ratio does inded have the shape of figure 1.

A second, parallel argument as to the validity of an Orr–Sommerfeld-type equation as a guide to the functional form of n_s can be seen by using a procedure first suggested by Synge (1938) whereby the Orr–Sommerfeld equation (see Synge 1938; Lin 1955; Koppel 1964; Drazin & Reid 1982) is formally rewritten so as to exhibit

the instability function or growth rate n_s (we shall omit the superscripts L–T). The result is (see (24) below)

$$n_s(k) = A\tau_{12}(k) - \nu B(k), \tag{10}$$

which shows, as expected on physical grounds, that n_s is composed of two terms: a source term proportional to the shear τ_{12}, and a sink proportional to the viscosity ν. The Orr–Sommerfeld equation further predicts that the shear peaks near the walls (see figure 4.21 of Drazin & Reid 1982), thus implying that in that region energy is extracted from the mean flow and fed into turbulence. Experimentally, it is known (see figure 5.5 of Townsend 1976) that the main source of energy production, i.e. of $\epsilon(k)$, occurs precisely in that region. Thus, the Orr–Sommerfeld equation predicts correctly the physically important feature of a region of instability. There, the main physical process is intrinsically the same as the one that characterized the transition from laminarity to turbulence. That feature has thus survived even in the presence of turbulence, which one may hope can be accounted for by a process of renormalization, for which we shall propose two methods and show that they yield very similar results.

We choose a coordinate system in which the mean flow is in the x-direction with one wall of the channel at $y = -D$ and the other at $y = D$. Consider the well-known laminar Poiseuille profile (Townsend 1976) with $\mathscr{y} = y/D$,

$$U(y) = U_0^{\mathrm{L}}(1 - \mathscr{y}^2), \tag{11}$$

with $U_0^{\mathrm{L}} = \frac{3}{2}U_{\mathrm{m}}$, $U_{\mathrm{m}} = (D^2\Delta p/3\nu l)$, where $\Delta p/l$ is the pressure drop along the channel of width $2D$ (we have taken unit density).

Since U_0^{L} cannot be identified with the experimental value of the mean flow at midchannel, we must find a way to renormalize it so as to take into account the presence of turbulence. We begin by *defining* a linear Reynolds number R_{L}

$$R_{\mathrm{L}} = U_0^{\mathrm{L}} D/\nu. \tag{12}$$

Introducing the shear stress at the wall, $\tau_0 = D(\Delta p/l)$ and the corresponding Reynolds number $R_\tau = \tau_0^{\frac{1}{2}} D/\nu$, we find

$$R_{\mathrm{L}} = \tfrac{1}{2}R_\tau^2. \tag{13}$$

It remains to relate R_τ to the experimental $R_{\mathrm{exp}} = (U_0 D/\nu)$, where U_0 is the measured centreline (i.e. midchannel) velocity. To do so, recall that the ratio R_{exp}/R_τ can be expressed alternatively as (see Clark 1968; Hussain & Reynolds 1975; Monin & Yaglom 1975) ($\kappa = 0.41$, $B = 5.1$)

$$\frac{1}{\kappa}\ln R_\tau + B, \quad 9.268\, R_{\mathrm{exp}}^{0.089}, \quad 25 + 3.5\times 10^{-3} R_\tau. \tag{14a, b, c}$$

The renormalization of U_0^{L}, or equivalently of R_{L}, is now complete since all the terms can be expressed in terms of R_{exp}.

A second approach for renormalizing the laminar profile can be devised by considering that the experimentally measured mean velocity field, $U(y)$, does indeed retain some vestiges of the laminar profile in the region near the walls where the energy is being produced. This can be seen by recalling the experimental form of $U(y)$ as given for example in Monin & Yaglom (1975), i.e.

$$U(y) = U_\tau R_\tau(1 - |\mathscr{y}|), \quad R_\tau(1 - |\mathscr{y}|) \leqslant 10, \tag{15a, b}$$

$$U(y) = U_\tau(\tfrac{5}{2}\ln R_\tau(1 - |\mathscr{y}|) + 5.1), \quad R_\tau(1 - |\mathscr{y}|) > 10, \tag{16a, b}$$

R_{exp}	R_τ	R_m	r_1	r_2
10^4	500	8735	12.55	9.54
2×10^4	925	17659	21.00	16.15
3×10^4	1331	26633	29.00	22.20

TABLE 1. Numerical results showing a comparison between the renormalizations (13) and (18)

and figure 5.5 of Townsend (1976) which shows that the maximum production occurs at the point where the linear regime changes to the logarithmic one. To renormalize the profile (11), we must eliminate the pressure gradient in terms of some other physical characteristic of the turbulent regime. We shall proceed as follows: Since both the profile (11) and the experimental one given by (16) are linear in the region where energy is being produced most efficiently, we shall require that the slope of the two functions be the same as y goes to $-D$ so as to assure that the two are identical in that region. This implies that $\Delta p/l = U_\tau^2/D$, which in turn implies that

$$U(y) = U_0^R(1-y^2), \tag{17}$$

with $U_0^R = (\nu R_\tau^2/2D)$. In this case we note that the renormalization for U_0^L is given by

$$U_0^L \to U_0^R = \frac{1}{3}\frac{R_\tau^2}{R_m} U_0^L. \tag{18}$$

In table 1, we present some numerical results that show how the two renormalizations, (13) and (18), yield similar results ($r_1 = R_m^3/72$, $r_2 = R_\tau^2/3R_m$). Considering the empirical nature of some of the relations employed in the previous derivation, the agreement of the results calculated using the two methods may be considered quite good.

It is probably not a coincidence that for $R_{exp} = 10^4$, we get a renormalization factor that is very close to the one first obtained by Reynolds & Tiederman (1967) more than twenty years ago and recently reconfirmed by Ierley & Malkus (1988). Both studies point out that the use of the experimental form of $U_{exp}(y, R_{exp})$ in the Orr–Sommerfeld equation yields stable solutions, i.e. $n_s < 0$, *if* it is assumed that the Reynolds number appearing explicitly in the Orr–Sommerfeld equation, R_{OS}, which is in effect a viscosity, is the same as the R_{exp} entering $U_{exp}(y, R_{exp})$. On the other hand, if R_{OS} is left as a free parameter, unstable solutions ($n_s > 0$) can be obtained if

$$R_{OS} \sim (10-15)\, R_{exp}. \tag{19}$$

In conclusion, the rate n_s entering in (2) is not the rate that characterizes the transition from laminarity to turbulence. Rather, it represents the rate at which energy is pumped into the system in a fully turbulent regime. In the case of channel flow, a region can be isolated near the walls where there is an instability in the sense that the energy is being extracted from the mean flow and given to the turbulence. In that region, the velocity profile is linear. We have tried to extract information about the rate at which such energy is transferred from one type of flow to the other by using the Orr–Sommerfeld equation in which, however, the strength of the mean flow was adjusted to match the experimental one. In that sense, the Orr–Sommerfeld equation must be viewed more as a phenomenological tool rather than the exact equation that it really is when one deals with the very different problem of the transition between laminarity and turbulence.

5. Solution of the Orr–Sommerfeld equation

We now proceed to show how the growth rate n_s can be computed from the solution of the well known Orr–Sommerfeld equation (see Synge 1938; Lin 1955; Koppel 1964; Drazin & Reid 1982). Measuring lengths in terms of the channel half-width, D, and velocities in terms of the laminar centreline mean velocity, U_0^L, the Orr–Sommerfeld equation can be written as

$$\frac{1}{i\alpha R_L}(\mathscr{D}^2-\tilde{\alpha}^2)^2 v(y) = (\mathscr{U}(y)-c)(\mathscr{D}^2-\tilde{\alpha}^2)v(y) - U''(y)v(y), \tag{20}$$

where $\mathscr{D} = \mathrm{d}/\mathrm{d}y$, $\alpha = k_x D$, $\tilde{\alpha} = k_\perp D$, $y = y/D$, $\mathscr{U} = U/U_0^L$, $c = c/U_0^L$, k is the wavenumber, $k_\perp^2 = k_y^2 + k_z^2$, and c is the complex phase speed. In deriving (20), the mean flow was taken to be in the x-direction and the channel is bounded by two infinite plane-parallel walls at $y = \pm D$.

For a Poiseuille flow, $\mathscr{U}(y) = 1-y^2$ is used and the boundary conditions $v = \mathrm{d}v/\mathrm{d}y = 0$ are imposed at $y = \pm 1$. If we further define $\tilde{R}_L$ by $\alpha R_L = \tilde{\alpha}\tilde{R}_L$, we obtain

$$\tilde{R}_L = \frac{R_L k_x}{(k_x^2+k_z^2)^{\frac{1}{2}}} = R_L \cos\phi, \tag{21}$$

then the solution of (20) yields for a given $\tilde{R}_L$ the complex eigenvalue c as a function of $\tilde{\alpha}$. Actually, for a given $\tilde{\alpha}$, there is a large number of discrete complex eigenvalues c. However, only one of the c has a positive imaginary part for some range of $\tilde{\alpha}$ which leads to growth of the instability. Defining the growth rate $n_s = k_x \mathrm{Im}\,(c)$ (where Im stands for the imaginary part of the enclosed function), the solution of (20) yields

$$n_s = \frac{U_0^L}{D}\tilde{\alpha}\,\mathrm{Im}\,(c)\cos\phi \;\; vs.\;\; \tilde{\alpha}, \tag{22}$$

for a given value of $\tilde{R}$. One can easily see that the maximum value of n_s (the most dangerous mode) corresponds to taking $\cos\phi = 1$, i.e. $k_z = 0$. To compare our results with experimental data, we need to change the velocity normalization from tne undisturbed centreline mean velocity, U_0^L, to the experimental centreline mean velocity U_0. This is done by multiplying (22) by $U_0/U_0^L = R_{exp}/R_L$. Hence, the desired growth rate is

$$\frac{n_s}{n_*} \;\; vs.\;\; k_\perp D, \quad \text{where} \quad n_* = \frac{U_0}{D}, \tag{23}$$

for different values of R_L or, equivalently, of $R_{exp} = U_0 D/\nu$.

6. Determination of k_y^2

Equation (23) is not yet the final result, for it gives n_s as a function of $k_\perp$. However, since homogeneity has been assumed in the application of the DIA and in the construction of the GISS model, they require the knowledge of the growth rate as a function of the total wavenumber, k. Channel flow is inhomogeneous in the direction perpendicular to the channel walls (the y-direction) so that an application of the model equations requires the construction of a wavenumber in the y-direction, i.e. $k_y = k_y(k_\perp)$. The application of a model which assumes homogeneity to a manifestly inhomogeneous flow may be criticized on first principles, yet we have learned from Leslie's (1973) work that the problem is analytically a very difficult one and trade-offs must be made to simplify it in order to make it solvable. We have kept as much

as possible of the essential physics in the model intact, consistent with the necessity of keeping the problem solvable. One of these trade-offs is our inability to describe the variation in the details of the flow in the y-direction. All of our calculated bulk properties represent an average of these properties over the inhomogeneous direction. We therefore proceed to find a suitable relationship between k_y and $k_\perp$. Following the original work of Synge (1938), we multiply the Orr–Sommerfeld equation (20) from the left by v^* (where the * denotes complex conjugation) and integrate the result over y from $-D$ to $+D$. Separating the real and imaginary parts, one obtains for the growth rate, $n_s = k_x \operatorname{Im}(c)$, the expression

$$n_s = \frac{k_x \operatorname{Im}(Q)}{I_1^2 + k_\perp^2 I_0^2} - \nu \frac{I_2^2 + 2k_\perp^2 I_1^2 + k_\perp^4 I_0^2}{I_1^2 + k_\perp^2 I_0^2}, \tag{24}$$

where

$$\operatorname{Im}(Q) = -\frac{1}{2}\int_{-D}^{D} U'[k_x(uv^* + u^*v) + k_z(vw^* + v^*w)]\,\mathrm{d}y \tag{25}$$

and

$$I_n^2 = \int_{-D}^{D} \left|\frac{\mathrm{d}^n v}{\mathrm{d}y^n}\right|^2 \mathrm{d}y. \tag{26}$$

Equations (24)–(26) have a simple physical interpretation. The first term on the right of (24) is a 'production term', since it provides the interaction between the shear $s = U'(y)$ in the mean flow and the Reynolds stress tensor: it gives a positive contribution to n_s. The second term is proportional to the viscosity, ν, and is always negative. It must clearly dominate at very large wavenumbers where the only remaining physical mechanism is kinematic viscosity. As we know, the latter enters the Navier–Stokes equations in the form $-\nu k^2$. On that basis, we shall therefore identify the coefficient of ν with k^2, i.e.

$$k^2 = k_y^2 + k_\perp^2 = \frac{I_2^2 + 2k_\perp^2 I_1^2 + k_\perp^4 I_0^2}{I_1^2 + k_\perp^2 I_0^2},$$

which, after some rearrangements, yields the desired result

$$k_y^2 = \frac{I_2^2 + k_\perp^2 I_1^2}{I_1^2 + k_\perp^2 I_0^2}, \tag{27}$$

which we shall use to generate the wavenumber k_y from the solutions of the Orr–Sommerfeld equation. For the fastest growing mode ($\cos\phi = 1$), (27) becomes

$$k_y^2 = \frac{\displaystyle\int_{-1}^{1} (u^*\mathscr{D}^2 u + v^*\mathscr{D}^2 v)\,\mathrm{d}\mathscr{y}}{\displaystyle\int_{-1}^{1} (u^*u + v^*v)\,\mathrm{d}\mathscr{y}}. \tag{28}$$

This result is intuitively appealing since k_y^2 is found to be the average of the operator $\mathrm{d}^2/\mathrm{d}y^2$ over the flow in the y-direction. The numerical results of table 3 lend themselves to an interesting physical interpretation since one can notice that

$$k_y \propto R_L^{\frac{1}{3}}, \tag{29}$$

where we have used (13) and (14) to translate the values of R_{exp} of table 3 into R_L. It is well known (see Drazin & Reid 1982, figure 4.5) that the width of the viscous sublayer is proportional to $R_L^{-\frac{1}{3}}$ and (29) confirms this fact, lending physical support to the derivation of k_y we have suggested and to the transition from R_L to R_{exp} as suggested by (13) and (14).

$R_{exp} = 12300$		$R_{exp} = 28600$		$R_{exp} = 30800$		$R_{exp} = 50000$	
kD	$10n_s/n_*$	kD	$10n_s/n_*$	kD	$10n_s/n_*$	kD	$10n_s/n_*$
8.631	0.125	10.533	0.173	10.700	0.168	12.74	0.410
9.081	0.291	11.265	0.414	11.256	0.356	14.51	0.838
9.588	0.447	12.113	0.643	11.886	0.537	16.37	1.19
10.144	0.589	13.053	0.849	12.578	0.709	18.85	1.41
10.739	0.713	14.068	1.025	13.323	0.867	21.33	1.42
11.369	0.813	15.147	1.158	14.112	1.006	24.0	1.08
12.031	0.886	16.285	1.234	14.940	1.123	27.1	0.117
12.721	0.927	17.479	1.254	15.804	1.212	—	—
13.441	0.930	18.732	1.183	16.702	1.268	—	—
14.189	0.889	20.053	1.003	7.634	1.283	—	—
14.972	0.796	—	—	18.599	1.251	—	—
15.794	0.645	—	—	19.603	1.160	—	—
—	—	—	—	20.650	0.998	—	—

TABLE 2. The growth rate $n_s(k)$ *vs.* k from a solution of the Orr–Sommerfeld equation for four values of the Reynolds number, R_{exp}. (The unit n_* is given by (23).)

$R_{exp} = 12300$		$R_{exp} = 30800$		$R_{exp} = 50000$	
$k_\perp D$	$k_y D$	$k_\perp D$	$k_y D$	$k_\perp D$	$k_y D$
0.453	8.62	0.425	13.3	0.32	12.7
0.48	9.07	0.485	15.8	0.36	14.5
0.507	9.58	0.505	16.7	0.40	16.6
0.533	10.1	0.525	17.6	0.44	18.8
0.56	10.7	0.545	18.6	0.48	21.3
0.587	11.4	0.565	19.6	0.52	24.0
0.613	12.0	0.585	20.6	0.56	27.1
0.64	12.7	0.605	21.7	—	—
—	—	0.625	22.9	—	—

TABLE 3. k_y as a function of $k_\perp$ computed from (28) for three values of the Reynolds number

7. The results for $n_s(k)$ and k_y

We have solved the Orr–Sommerfeld equation (20) for four values of R_{exp}: 12300, 28600, 30800 and 50000. The first three values correspond to the experimental values of Laufer (1951) and Hussain & Reynolds (1975). In table 2, we present the values of $n_s(k)$ in units of n_*, equation (23), as a function of the dimensionless wavenumber kD and in table 3 we give the values of k_y *vs.* $k_\perp$. In figure 2, we plot n_s/n_* *vs.* kD for different values of the Reynolds number.

8. Solutions of the turbulence equations

The function $n_s(k)$ was used to solve both the DIA and the GISS models, (1)–(5) and (7)–(8). In each case, we computed several quantities of interest that we discuss below.

(i) Turbulent energy spectral function, $F(k)$. In figure 3 we plot

$$F(k)/F_* \text{ vs. } kD, \quad F_* = U_0^2 D = (\nu^2/D) R_{exp}^2, \tag{30}$$

calculated using the GISS model. In figure 4, we compare the GISS and DIA results.

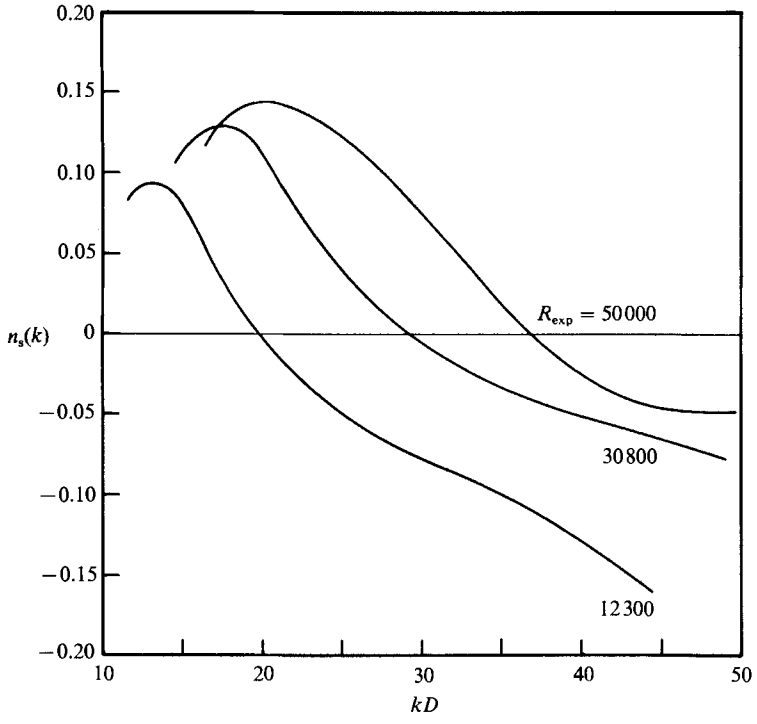

FIGURE 2. The growth rate $n_s(k)$ *vs.* k in units of n_*, equation (23), as solution of the Orr–Sommerfeld equation for $R_{exp} = 12300$, 30800, and 50000.

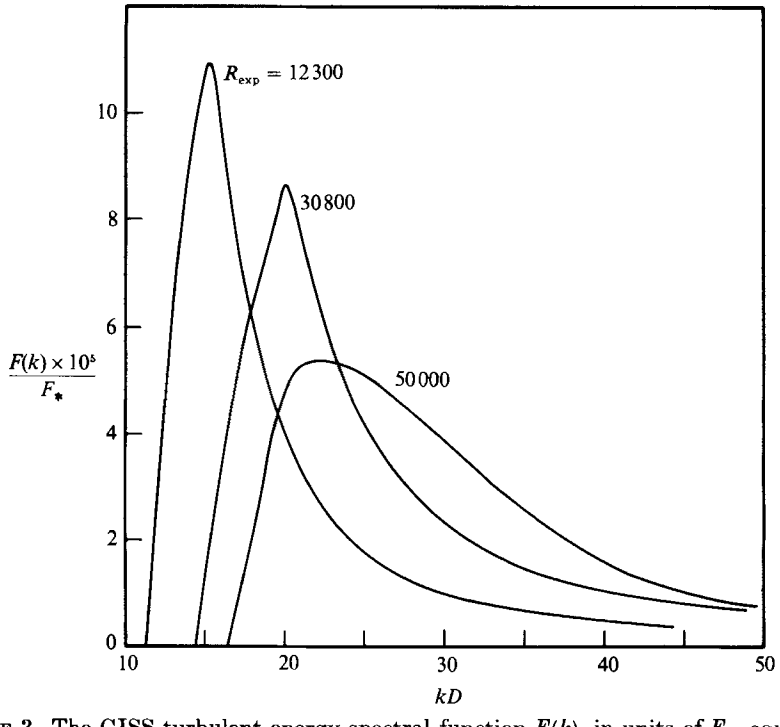

FIGURE 3. The GISS turbulent energy spectral function $F(k)$, in units of F_*, equation (30), *vs.* k for $R_{exp} = 12300$, 30800, and 50000.

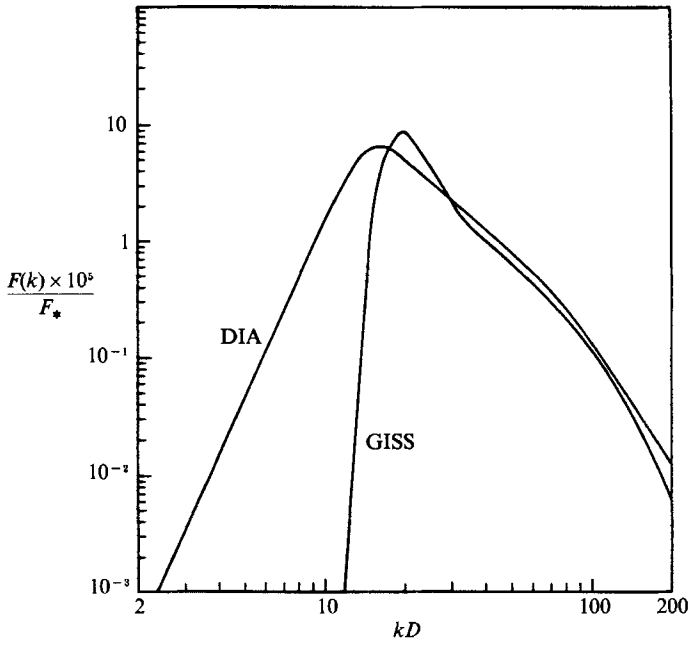

FIGURE 4. A comparison of the GISS and DIA spectral functions for $R_{\exp} = 30800$. (Same units as in figure 3.)

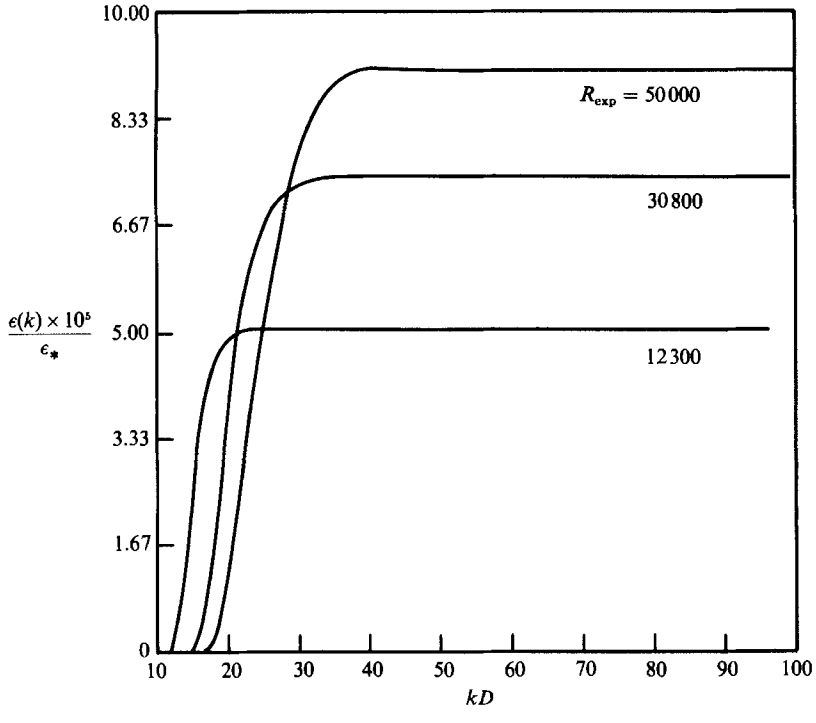

FIGURE 5. The energy $\epsilon(k)$ per unit mass and time, equation (2), in units of ϵ_*, equation (31), for several values of $R_{\exp}$. It can be seen that the function saturates very rapidly, thus becoming independent of the wavenumber k.

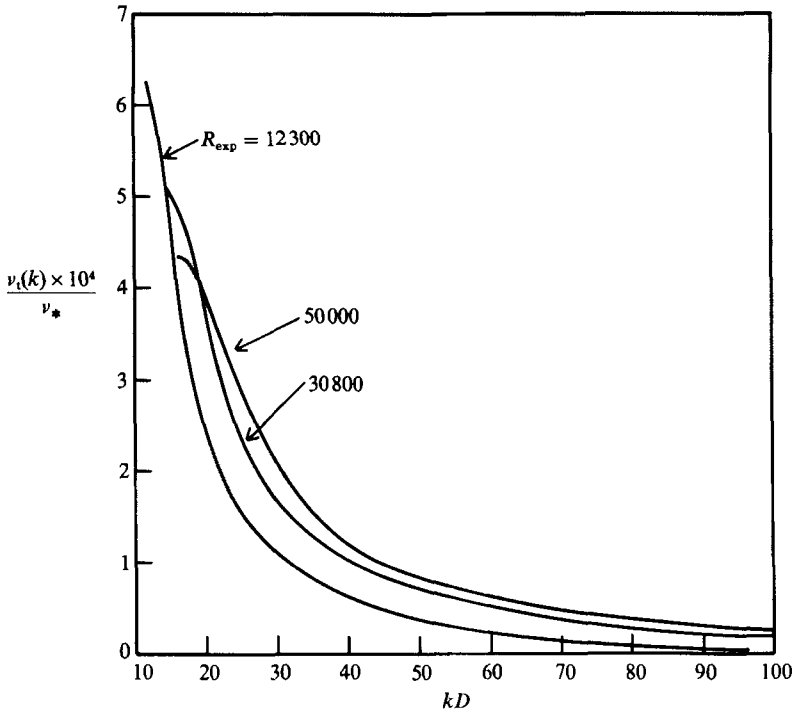

FIGURE 6. The turbulent viscosity $\nu_t(k)$ *vs.* k, equation (4), in units of ν_*, equation (32), for several values of R_{exp}.

(ii) The energy $\epsilon(k)$. In figure 5 we plot the quantity

$$\epsilon(k)/\epsilon_* \; vs. \; kD, \quad \epsilon_* = U_0^3/D = (\nu^3/D^4)R_{exp}^3, \tag{31}$$

where $\epsilon(k)$ is defined in (2). (The physical units of ϵ are erg g^{-1} s^{-1}.)

(iii) The turbulent viscosity, $\nu_t(k)$. In figure 6 we plot

$$\nu_t(k)/\nu_* \; vs. \; kD, \quad \nu_* = U_0 D = \nu R_{exp}, \tag{32}$$

where $\nu_t(k)$ is the turbulent viscosity defined in (4). The largest value of the turbulent viscosity is attained at $k = k_0$, where k_0 is the smallest allowed wavenumber. Taking the limit $k \to k_0$ in (1), we obtain

$$\nu_t(k_0) = \frac{n_s(k_0)}{k_0^2}. \tag{33}$$

(iv) One-dimensional spectra. Both Laufer (1951) and Hussain & Reynolds (1975) present their experimental results in terms of the one-dimensional spectral energy function defined in terms of the three-dimensional $F(k)$ as follows (see Hinze 1975, equations 3.72, 3.48. 3.47):

$$E_1(k_1) = \frac{1}{2}\int_{k_1}^{\infty} k^{-1}F(k)\,(1 - k_1^2/k^2)\,\mathrm{d}k. \tag{34}$$

We have computed $E_1(k_1)$ for the case corresponding to the experimental condition in the Hussain and Reynolds paper, i.e. $R_{exp} = 28600$, $U_0 = 1350$ cm s^{-1}, $D = 3.18$ cm. The results are presented in figure 7.

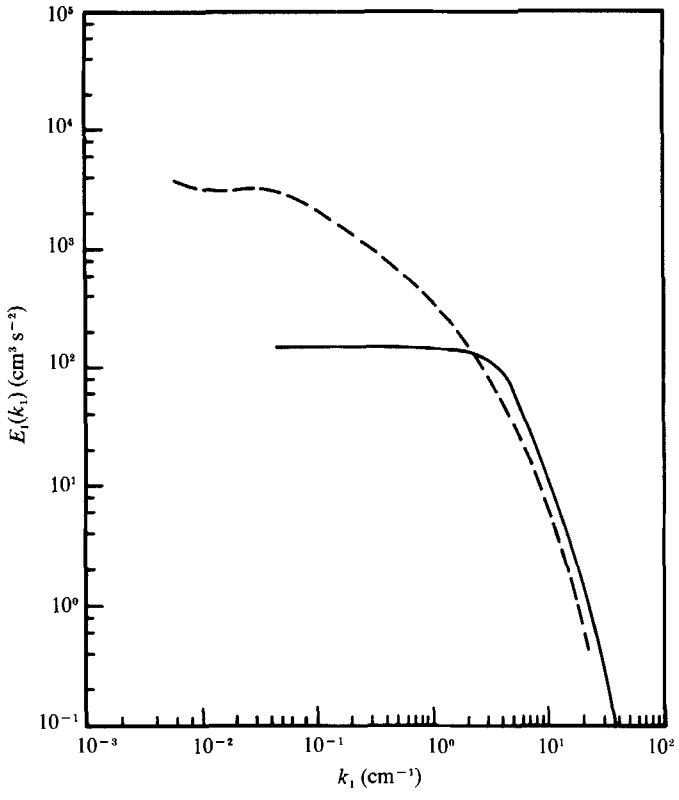

FIGURE 7. Comparison of the theoretical one-dimensional spectral function, equation (34), *vs.* k_1 (full line), with the one measured by Hussain & Reynolds (1975) for $R_{\exp} = 28600$, $U_0 = 1350$ cm s^{-1} and $D = 3.18$ cm.

On the other hand, Laufer (1951) presents his experimental data in terms of the function

$$F_{\overline{u}^2}(n) = \frac{2\pi}{U_0} E_1(k_1) \left(\int_0^\infty E_1(k_1)\, \mathrm{d}k_1 \right)^{-1}, \tag{35}$$

where $2\pi n = k_1 U_0$. The comparison between Laufer's measured spectrum ($R_{\exp} = 30800$, $U_0 = 728$ cm s^{-1}, $D = 6.35$ cm) and the theoretical results is presented in figure 8.

(v) Turbulent velocities and scales of turbulence. Laufer (1951) and Hussain & Reynolds (1975) also provide experimental data for other quantities of interest, namely

(*a*) turbulent energy

$$\langle u^2 \rangle = \int_0^\infty F(k)\, \mathrm{d}k, \tag{36}$$

(*b*) turbulent velocity

$$\langle u_x^2 \rangle^{\frac{1}{2}} = \langle u_y^2 \rangle^{\frac{1}{2}} = \langle u_z^2 \rangle^{\frac{1}{2}} = (\tfrac{1}{3} \langle u^2 \rangle)^{\frac{1}{2}}, \tag{37}$$

(*c*) Taylor microscale λ_x

$$\lambda_x^2 = \int_0^\infty E_1(k_1)\, \mathrm{d}k_1 \left(\int_0^\infty k_1^2 E_1(k_1)\, \mathrm{d}k_1 \right)^{-1}, \tag{38}$$

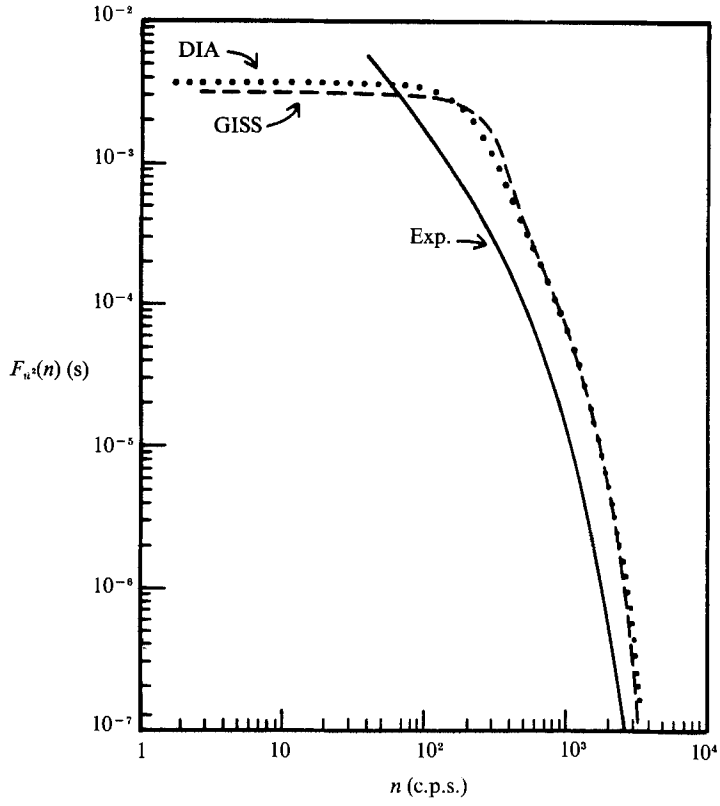

FIGURE 8. Comparison of the theoretical one-dimensional spectral function defined by (35) with the one measured by Laufer (1951), corresponding to $R_{exp} = 30800$, $U_0 = 728$ cm s^{-1} and $D = 6.35$ cm.

	$R_{exp} = 12300$			$R_{exp} = 30800$			$R_{exp} = 50000$
	GISS	DIA	Exp.	GISS	DIA	Exp.	GISS
$\langle u^2\rangle \times 10^3$	0.920	1.14	—	1.16	1.21	—	1.25
$\langle u_x^2\rangle^{\frac{1}{2}} \times 10^2$	1.75	1.95	3.6	1.96	2.01	3.0	2.00
$\nu_t \times 10^4$	6.30	—	—	5.04	—	—	4.30
$\epsilon \times 10^5$	4.70	5.43	—	7.12	7.53	3.62	9.08
λ_x	0.192	0.092	0.11	0.053	0.051	0.095	0.141
Λ_x	0.857	1.05	—	0.69	0.80	0.63	0.49
$l_0 \times 10^3$	10.3	9.97	—	4.70	—	—	—

TABLE 4. Turbulent velocities and scales of turbulence

(*d*) turbulence macroscale Λ_x

$$\Lambda_x = \frac{3\pi}{4}\int_0^\infty k_1^{-1} E_1(k_1)\,\mathrm{d}k_1 \Big(\int_0^\infty E_1(k_1)\,\mathrm{d}k_1\Big)^{-1}, \tag{39}$$

(*e*) Kolmogorov scale l_0

$$l_0 = (\nu^3/\epsilon)^{\frac{1}{4}}. \tag{40}$$

In table 4, we present $\langle u^2\rangle$ in units of U_0^2, $\langle u_x^2\rangle^{\frac{1}{2}}$ in units of U_0, $\nu_t = \nu_t(k_0)$ in units of $U_0 D$, ϵ in units of U_0^3/D, and λ_x, Λ_x, and l_0 in units of D. Experimental data are included where available.

9. Pressure fluctuations in a turbulent channel flow

We begin by considering that in an incompressible fluid, the pressure $p(\boldsymbol{x})$ is given by the solution of the Poisson's equation

$$\nabla^2 p(\boldsymbol{x}) = -\rho \frac{\partial^2 v_i(\boldsymbol{x})\, v_j(\boldsymbol{x})}{\partial x_i\, \partial x_j}, \tag{41}$$

where $\boldsymbol{v}(\boldsymbol{x})$ is the total velocity, ρ is the constant density, and the summation convention has been employed. If, as usual, one splits v_i into a fluctuating part u_i and a mean field U_i, the right-hand side of (41) is seen to contain three contributions: a term in $u_i u_j$, one in the form $u_i U_j$, and one in $U_i U_j$. Following Kraichnan (1956*a*, *b*), we shall assume that the cross-term is much smaller than the other two so that from the solution of (41), one can construct the fluctuating pressure, i.e.

$$\frac{\langle p^2 \rangle}{\rho^2} = \int \mathrm{d}^3\boldsymbol{k}[\Pi_{\mathrm{T\text{-}T}}(\boldsymbol{k}) + \Pi_{\mathrm{T\text{-}M}}(\boldsymbol{k})] \equiv \int \mathrm{d}^3\boldsymbol{k}\Pi(\boldsymbol{k}), \tag{42}$$

where T–T indicates the contribution arising from the turbulence–turbulence interaction and T–M indicates the one arising from the interaction between the turbulence and the mean flow. It is a fact, which we have verified numerically, that

$$\Pi_{\mathrm{T\text{-}M}} \gg \Pi_{\mathrm{T\text{-}T}}. \tag{43}$$

The expression for $\Pi_{\mathrm{T\text{-}T}}$ was first evaluated by Batchelor (1951). The result is

$$4\pi\Pi_{\mathrm{T\text{-}T}}(\boldsymbol{k}) = \iint E(k')\, E(k-k') \frac{\sin^4\theta}{|\boldsymbol{k}-\boldsymbol{k}'|^4} k'^2\, \mathrm{d}k' \sin\theta\, \mathrm{d}\theta. \tag{44}$$

The expression for $\Pi_{\mathrm{T\text{-}M}}$ is much more difficult to compute. To treat the physical problem under consideration, we need an expression that depends not only on $\boldsymbol{k}$ but also on the coordinate variable across the channel of finite width Δ, i.e.

$$\Pi_{\mathrm{T\text{-}M}}(\boldsymbol{k}) \to \Pi_{\mathrm{T\text{-}M}}(\boldsymbol{k}, x_2; \Delta). \tag{45}$$

The only expression for $\Pi_{\mathrm{T\text{-}M}}$ available in the literature is due to Kraichnan (1956*b*) (his equation 5.20), which yields the pressure at the lower boundary of a semi-infinite medium (a flat plate), i.e.

$$\Pi_{\mathrm{T\text{-}M}}(\boldsymbol{k}, 0; \infty). \tag{46}$$

Since we plan to study the propagation of an electromagnetic beam in a channel flow, Kraichnan's expression is not applicable to our case. We shall therefore derive the expression for $\Pi_{\mathrm{T\text{-}M}}(\boldsymbol{k}, x_2) \equiv \Pi_{\mathrm{T\text{-}M}}(\boldsymbol{k}, x_2; \Delta)$.

Since in the case of a channel flow, two directions, say x_1 and x_3, in the plane of the mean flow can be considered to be homogeneous, one can perform a Fourier transform of (41) on the variables x_1, x_3, and t. Equation (41) then becomes

$$\frac{\partial^2 p(x_2, \boldsymbol{\kappa}, \omega)}{\partial x_2^2} - \kappa^2 p(x_2, \boldsymbol{\kappa}, \omega) = -T(x_2, \boldsymbol{\kappa}, \omega), \tag{47}$$

where $\kappa^2 = k_1^2 + k_3^2$, and

$$p(x_2, \boldsymbol{\kappa}, \omega) = (2\pi)^{-\frac{3}{2}} \int p(\boldsymbol{x}, t)\, \mathrm{e}^{-\mathrm{i}(k_1 x_1 + k_3 x_3 - \omega t)}\, \mathrm{d}x_1\, \mathrm{d}x_3\, \mathrm{d}t. \tag{48}$$

Equation (47) is a second-order, inhomogeneous differential equation whose solution can be written as

$$2\kappa p(x_2,\boldsymbol{\kappa},\omega) = \int_a^{x_2} \mathrm{d}x_2' \, \mathrm{e}^{-\kappa(x_2-x_2')}\, T(x_2',\boldsymbol{\kappa},\omega) - \int_b^{x_2} \mathrm{d}x_2' \, \mathrm{e}^{\kappa(x_2-x_2')}\, T(x_2',\boldsymbol{\kappa},\omega). \tag{49}$$

The two constants of integration a and b must be determined by imposing the boundary conditions

$$\frac{\mathrm{d}}{\mathrm{d}x_2} p(x_2,\boldsymbol{\kappa},\omega)\bigg|_{x_2=0,\,\Delta} = 0, \tag{50}$$

since the fluid is bounded by two walls at $x_2 = 0$ and $x_2 = \Delta = 2D$. The final result is

$$p(x_2,\boldsymbol{\kappa},\omega) = \int_0^{\Delta} \mathrm{d}x_2' \, g_2(x_2,x_2';\kappa)\, T(x_2') - \int_0^{x_2} \mathrm{d}x_2' \, g_1(x_2,x_2';\kappa)\, T(x_2'), \tag{51}$$

where, for the sake of simplicity, we have explicitly written only the x_2 dependence of T, i.e. $T(x_2) = T(x_2,\boldsymbol{\kappa},\omega)$, and where we have defined two functions g_1 and g_2 as

$$\kappa g_1(x_2,x_2';\kappa) = \sinh\kappa(x_2-x_2') \tag{52}$$

$$\kappa g_2(x_2,x_2';\kappa) = \frac{\cosh\kappa x_2}{\sinh\kappa\Delta}\cosh\kappa(\Delta-x_2'). \tag{53}$$

By taking the limit $\Delta\to\infty$ and $x_2\to 0$, (51) reduces to (3.9) of Kraichnan (1956*b*). (In the case $x_2 = 0$ and non-zero Δ, (51) does not reduce to (3.11) of Kraichnan (1956*b*) since the latter is missing a factor of 2 in front of the second term.) Equation (51) is the basic ingredient of our calculations since it gives the value of the fluctuating pressure at any given point in a channel of full width $\Delta = 2D$. From (51) we obtain, with a slight change of notation,

$$\begin{aligned}|p(x_2,\boldsymbol{\kappa},\omega)|^2 = {} & \int_0^{\Delta}\mathrm{d}x \int_0^{\Delta}\mathrm{d}y\, g_2(x_2,x;\kappa)\, g_2(x_2,y;\kappa)\,\langle T^*(x,\boldsymbol{\kappa},\omega)\, T(y,\boldsymbol{\kappa},\omega)\rangle \\ & -2\int_0^{\Delta}\mathrm{d}x \int_0^{x_2}\mathrm{d}y\, g_1(x_2,y;\kappa)\, g_2(x_2,x;\kappa)\,\langle T^*(x,\boldsymbol{\kappa},\omega)\, T(y,\boldsymbol{\kappa},\omega)\rangle \\ & +\int_0^{x_2}\mathrm{d}x \int_0^{x_2}\mathrm{d}y\, g_1(x_2,x;\kappa)\, g_1(x_2,y;\kappa)\,\langle T^*(x,\boldsymbol{\kappa},\omega)\, T(y,\boldsymbol{\kappa},\omega)\rangle,\end{aligned} \tag{54}$$

where the asterisk denotes complex conjugation and the angular brackets denote an ensemble average.

As is well known, the largest contribution to $T(x_2)$ comes from the interaction of the turbulent field with the mean flow, i.e.

$$T(\boldsymbol{x},t) = 2\rho s(x_2)\frac{\partial U_2}{\partial x_1}, \tag{55}$$

where the shear $s(x_2)$ is given by

$$s(x_2) = \frac{\partial U_1(x_2)}{\partial x_2}, \tag{56}$$

so that

$$\begin{aligned}\langle T(\boldsymbol{x},t)\, T(\boldsymbol{x}',t')\rangle &= S(x_2,x_2',x_1-x_1',x_3-x_3',t-t') \\ &= -4\rho^2 s(x_2)\, s(x_2')\frac{\partial^2}{\partial\zeta_1^2} R_{22}(x_2,x_2',\zeta_1,\zeta_3,t),\end{aligned} \tag{57}$$

where it has been explicitly indicated that in the directions x_1 and x_3 the fluid is

homogeneous, R_{22} is the two-point velocity correlation function, $\zeta_1 = x_1' - x_1$, and $\zeta_3 = x_3' - x_3$. Taking now

$$R_{22}(x_2, x_2', \zeta_1, \zeta_3, t) = (2\pi)^{-\frac{3}{2}} \int \mathrm{d}^2\,\boldsymbol{\kappa}\,\mathrm{d}\omega\,\mathrm{e}^{\mathrm{i}(\boldsymbol{\kappa}\cdot\boldsymbol{\zeta}+\omega t)} R_{22}(x_2, x_2', \boldsymbol{k}, \omega) \tag{58}$$

and using an analogous expansion for S, we have

$$S(x_2, x_2', \boldsymbol{\kappa}, \omega) = 4\rho^2 s(x_2)\, s(x_2')\, \kappa_1^2 R_{22}(x_2, x_2', \boldsymbol{\kappa}, \omega). \tag{59}$$

The relation between $\langle T^*(x, \boldsymbol{\kappa}, \omega)\, T(y, \boldsymbol{\kappa}, \omega)\rangle$ in (54) and the quantity $S(x_2, x_2, \boldsymbol{\kappa}, \omega)$ is (see Kraichnan 1956*b*)

$$\langle T^*(x, \boldsymbol{\kappa}, \omega)\, T(y, \boldsymbol{\kappa}, \omega)\rangle = (2\pi)^{-\frac{3}{2}} S(x_2, x_2', \boldsymbol{\kappa}, \omega).$$

Using the reality of $R_{22}(\boldsymbol{x}, t)$, we write

$$R_{22}(x_2, x_2', \boldsymbol{\kappa}, \omega) = \frac{(2\pi)^{\frac{1}{2}}}{\Delta} \sum_{n=-\infty}^{\infty} \cos k_2^{(n)}(x_2 - x_2')\, R_{22}(\boldsymbol{k}, \omega), \tag{60}$$

where $k_2^{(n)} = 2\pi n/\Delta$. Equations (57)–(60) are substituted in (54) and the result is integrated over all ω. Using the relations

$$\int_{-\infty}^{\infty} R_{22}(\boldsymbol{k}, \omega)\,\mathrm{d}\omega = (2\pi)^2\, \Phi_{22}(\boldsymbol{k}), \tag{61}$$

$$\Phi_{22}(\boldsymbol{k}) = \frac{E(k)}{4\pi k^4}\kappa^2, \tag{62}$$

where $E(k)$ is the velocity spectrum for homogeneous turbulence, and where

$$\langle p^2(x_2)\rangle = \int |p(x_2, \boldsymbol{k}, \omega)|^2\, \mathrm{d}^2\boldsymbol{\kappa}\,\mathrm{d}\omega, \tag{63}$$

we obtain, after a series of lengthy integrations over the variables x and y in (54), the final result

$$\frac{\langle p^2(x_2)\rangle}{\rho^2} = \int \mathrm{d}^3\boldsymbol{k}\, \Pi(\boldsymbol{k}, x_2), \tag{64}$$

where

$$\Pi(\boldsymbol{k}, x_2) = \frac{s_0^2}{\pi}\frac{2\pi}{\Delta} \sum_{n=-\infty}^{\infty} \delta(k_2 - k_2^{(n)}) \frac{E(k)}{k^4}\frac{k_1^2 k_2^2}{k^4}(\Gamma_1^2(\boldsymbol{k}, x_2) + \Gamma_2^2(\boldsymbol{k}, x_2)), \tag{65}$$

$$\Gamma_1(\boldsymbol{k}, x_2) = \frac{\cosh \kappa(\frac{1}{2}\Delta - x_2)}{\sinh \frac{1}{2}\kappa\Delta} + \frac{\kappa}{k_2^{(n)}}\left(1 - 2\frac{x_2}{\Delta}\right)\sin k_2^{(n)} x_2 - \frac{4\kappa}{k^2\Delta}\cos k_2^{(n)} x_2, \tag{66}$$

$$\Gamma_2(\boldsymbol{k}, x_2) = \frac{2}{k_2\Delta}\left(1 - 2\frac{\kappa^2}{k^2}\right)\frac{\sinh \kappa(\frac{1}{2}\Delta - x_2)}{\cosh \frac{1}{2}\kappa\Delta} + \frac{\kappa}{k_2^{(n)}}\left(1 - 2\frac{x_2}{\Delta}\right)\cos k_2^{(n)} x_2 + \frac{4\kappa}{k^2\Delta}\sin k_2^{(n)} x_2, \tag{67}$$

with $\delta(x)$ the Dirac delta function. To be consistent with the spirit of the model adopted in this paper, the velocity profile used in performing the integrations that lead to (64) was $U(x_2) = s_0 x_2(1 - x_2/\Delta)$, where $s_0 = \tau_0/\nu$. This gives for the shear

$$s(x_2) = s_0\left(1 - \frac{2}{\Delta}x_2\right). \tag{68}$$

However, it is clear that the above formalism is valid for any shear.

Using the spectral functions $E(k)$ derived from the DIA and the GISS model, we have computed the pressure spectral function $\Pi(\boldsymbol{k})$ and then integrated over all

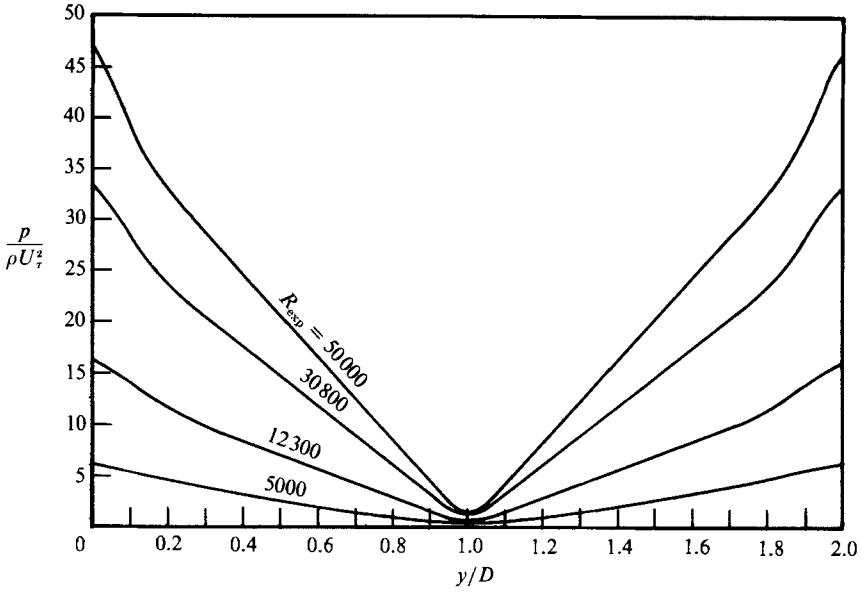

FIGURE 9. The value of the fluctuating pressure, in units of ρU_τ^2 computed from (64), as a function of distance across the channel of width $\Delta = 2D$. The results are computed using the GISS model.

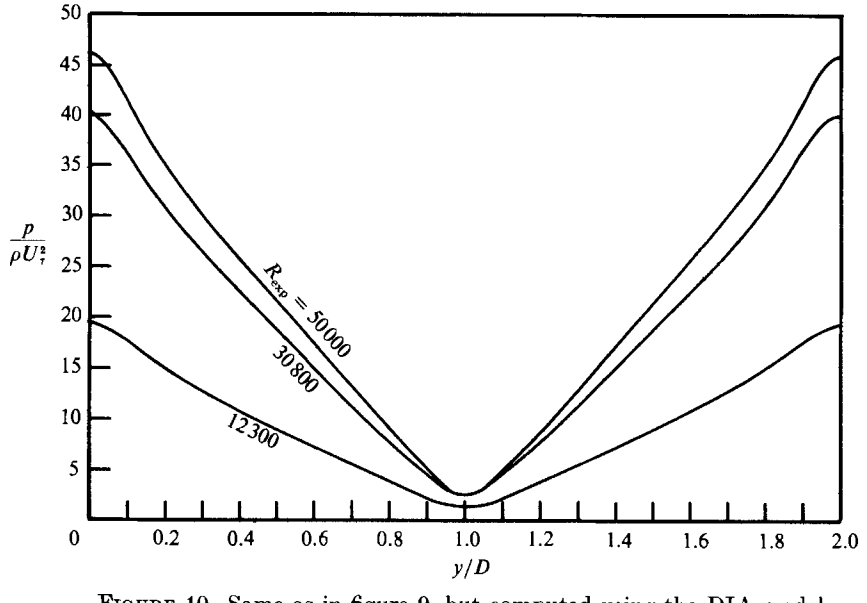

FIGURE 10. Same as in figure 9, but computed using the DIA model.

wavevectors $\boldsymbol{k}$. The resulting pressures, in units of ρU_τ^2, are presented in figures 9 and 10. As one can see, for $R_{\mathrm{exp}} = 5000$, the calculated value of the pressure at the wall is 6.31, while experiments of Blake (1970) and direct numerical simulation of Handler *et al.* (1984), yield a lower value, i.e. 3.22, the discrepancy being due most likely to anisotropy effects (see §11).

10. Propagation of electromagnetic waves in a turbulent channel flow

An important application of the previous formalism is to the case of propagation of a laser beam through a turbulent channel flow medium. Of primary importance is, for example, the evaluation of the degree of attenuation in the beam intensity I. Using the formalism developed by Hogge, Butts & Burlakoff (1974), the total beam intensity I, as a function of the coordinates x_0 and y_0 in the plane perpendicular to the direction of propagation, is given by

$$I(x_0, y_0) = \frac{A_0^2}{(\lambda f)^2} \exp(-\sigma_\phi^2) \int dx_1\, dx_2\, dy_1\, dy_2 \times \exp\left[C_\phi(\rho) - g - \frac{ip}{f}(x_0(x_1 - x_2) + y_0(y_1 - y_2))\right] \quad (69)$$

where $p = 2\pi/\lambda$ and

$$w_1^2 g \equiv x_1^2 + x_2^2 + y_1^2 + y_2^2, \quad \rho^2 \equiv (x_1 - x_2)^2 + (y_1 - y_2)^2, \quad (70)$$

Here, λ is the wavelength, f the focal distance, and w_1 the spot size. In (69), $C_\phi(\rho)$ is the phase autocorrelation function and σ_ϕ^2 its value at $\rho = 0$. By separating the integrand in (69) so as to exhibit the coherent and incoherent parts of the total intensity, one can then evaluate the corresponding powers obtained by integrating the intensity over the variables x_0 and y_0. A simple integration then gives the exact result

$$P = P_{\text{inc}}/P_{\text{total}} = 1 - \exp(-\sigma_\phi^2), \quad (71)$$

which is often written as

$$P = \sigma_\phi^2/(1 + \sigma_\phi^2), \quad (72)$$

since in most cases σ_ϕ^2 is smaller than unity. The quantity $\sigma_\phi^2 = C_\phi(0)$ is defined in Tatarskii (1961) as

$$\sigma_\phi^2 = p^2 \int d^3\boldsymbol{k} \int_0^L d\xi' \int_0^L d\xi'' \cos(k_2(\xi' - \xi'')) \cos(\omega(L - \xi')) \cos(\omega(L - \xi'')) \Phi_n(\boldsymbol{k}, x', x'') \quad (73)$$

where

$$\omega = \frac{k_\perp^2}{2p}, \quad \kappa^2 = k_1^2 + k_3^2, \quad k^2 = k_2^2 + \kappa^2, \quad (74)$$

the ξ' and ξ'' integrations are over the photon optical path of length L, which is related to the full channel width $2D$, $x' = (2D/L)\xi'$, and $x'' = (2D/L)\xi''$. One of the integrations over optical path in (73) can be done by changing variables to sum and difference coordinates, $\frac{1}{2}(\xi' + \xi'')$ and $\xi' - \xi''$. We then assume that Φ_n is a locally isotropic field, i.e. a function only of the sum coordinates, so that the integration over the difference coordinates can be done analytically.

The function Φ_n is defined as the spectral function of the square of the refractive index fluctuations, i.e. for mean flow in the x_1 direction with the coordinate system oriented such that x_2 is the coordinate variable spanning the channel with $0 \leqslant x_2 \leqslant \Delta = 2D$, we have

$$\langle n'^2(x_2) \rangle = \int d^3\boldsymbol{k} \Phi_n(\boldsymbol{k}, x_2), \quad (75)$$

where we have taken from Monin & Yaglom (1975) that

$$n = 1 + n' = 1 + \alpha p, \quad \alpha = 7.9 \times 10^{-8} g(\lambda)/T. \quad (76)$$

Here the pressure p is measured in c.g.s. units and the temperature T in K. The

slight dependence on the wavelength λ is represented by the function $g(\lambda)$, where $g(\lambda = 1\mu) = 1$, $g(\lambda = 0.5\mu) = 1.02$, and $g(\lambda = 0.2\mu) = 1.18$. It then follows that

$$\langle n'^2(x_2)\rangle = (\alpha\rho)^2 \frac{\langle p^2(x_2)\rangle}{\rho^2} = \int \Phi_n(\boldsymbol{k}, x_2)\, \mathrm{d}^3\boldsymbol{k}, \tag{77}$$

where ρ is the density in c.g.s. units. Using (42), it follows that

$$\Phi_n(\boldsymbol{k}, x_2) = (\alpha\rho)^2 \Pi(\boldsymbol{k}, x_2). \tag{78}$$

10.1. *The quantity* $\rho\alpha U_0^2$

Using the equation of state and the sound speed c_s

$$p = \frac{kN_A}{\mu}\rho T = \frac{8.32 \times 10^7}{\mu}\rho T, \quad c_s^2 = \gamma\frac{p}{\rho}, \tag{79}$$

where k is Boltzmann's constant, N_A is Avogadro's number, μ the molecular weight (gm/mole), and γ the ratio of specific heats, we derive using (76)

$$\rho\alpha U_0^2 = \gamma_* M^2, \tag{80}$$

where the constant γ_* (ρ is in c.g.s. units) and the Mach number M are defined as

$$\gamma_* \equiv 6.5696\gamma\rho/\mu, \quad M \equiv U_0/c_s. \tag{81}$$

10.2. *The results*

In table 5, we present the values of 10^2P, equation (71), calculated using (73), (78), and (65). The spectral function $E(k)$ is calculated using both the GISS model and the DIA. For each entry, R_{exp} and M, the corresponding U_0, D (the channel half-width), and L (optical path) can be computed from the following relations (p in atmospheres and ρ in c.g.s. units)

$$U_0(\mathrm{cm/s}) = c_s M = 10^3 M(\gamma p/\rho)^{\frac{1}{2}}, \quad D(\mathrm{cm}) = \frac{\nu}{U_0}R_{exp}, \quad L(\mathrm{cm}) = 2(1+n_r^2)^{\frac{1}{2}}D(\mathrm{cm}).$$

The values of the viscosity ν (in $\mathrm{cm^2\ s^{-1}}$), density ρ (in $\mathrm{g\ cm^{-3}}$), and the refractive index n_r are given in table 5 caption. A plot of 10^2P versus the Mach number is displayed in figure 11 for $\Delta = 2$, 3, and 5 mm.

11. Anisotropy

One possible reason for the discrepancy between the calculated and measured values of the pressure fluctuations at the wall is the lack in our calculation of the inclusion of anisotropy effects induced by the mean flow. This may also be the cause of the discrepancy between the calculated and observed one-dimensional energy spectra. Kraichnan (1956*a*) suggested a simple model for an elongated eddy structure via a constant scale change in the direction of the mean flow. This simple model will be generalized here in order to judge what qualitative effect anisotropy would have on the one-dimensional energy spectrum.

We introduce a scale transformation for the wavenumber variables

$$k_1' = \frac{k_1}{\alpha(k')}, \quad k_2' = k_2, \quad k_3' = k_3, \tag{83}$$

M	Δ	GISS	DIA
	$R_{exp} = 12300$		
0.1	5.71	6.50×10^{-4}	1.04×10^{-3}
0.114	5.00	8.49×10^{-4}	1.36×10^{-3}
0.190	3.00	2.36×10^{-3}	3.77×10^{-3}
0.2	2.86	2.59×10^{-3}	4.16×10^{-3}
0.286	2.00	5.30×10^{-3}	8.48×10^{-3}
0.3	1.90	5.82×10^{-3}	9.35×10^{-3}
0.4	1.43	1.04×10^{-2}	1.66×10^{-3}
0.5	1.14	1.62×10^{-2}	2.59×10^{-2}
0.6	0.952	2.33×10^{-2}	3.72×10^{-2}
0.7	0.816	3.23×10^{-2}	5.07×10^{-2}
	$R_{exp} = 30800$		
0.1	14.3	9.04×10^{-3}	1.81×10^{-2}
0.2	7.15	3.56×10^{-3}	7.23×10^{-2}
0.286	5.00	7.38×10^{-2}	0.148
0.3	4.77	8.08×10^{-2}	0.162
0.4	3.58	0.144	0.289
0.477	3.00	0.205	0.410
0.5	2.86	0.225	0.450
0.6	2.38	0.324	0.649
0.7	2.04	0.438	0.883
0.715	2.00	0.459	0.920
	$R_{exp} = 50000$		
0.1	23.2	3.33×10^{-2}	4.30×10^{-2}
0.2	11.6	0.133	0.183
0.3	7.74	0.297	0.413
0.4	5.81	0.530	0.734
0.465	5.00	0.714	0.987
0.5	4.65	0.827	1.14
0.6	3.87	1.19	1.64
0.7	3.32	1.59	2.23
0.774	3.00	1.97	2.71
1.16	2.00	4.35	5.99

TABLE 5. Values of $10^2 P$, equation (71), and full channel width Δ (in mm) for different Mach and Reynolds numbers. Gas properties: $\nu = 8.6 \times 10^{-2}$ cm^2 s^{-1}, $\rho = 2.07 \times 10^{-3}$ g cm^{-3}, $p = 2$ atm, $\mu = 28$ g mole^{-1}. Optical properties: wavelength $\lambda = 0.53$ μm, refractive index $n_r = 1.53$.

where 1 is the streamwise direction, 2 is the direction across the channel, and $\alpha(\boldsymbol{k}')$ is a scale function. The primed variables, i.e. those for which the scales are stretched in the streamwise direction, are the physical variables. Since we only know $E(k)$ for the isotropic case (in which there is no stretching), we derive a relationship between the velocity covariance tensors in the primed and unprimed systems. For homogeneous and isotropic turbulence, the velocity correlation function $\Phi_{ij}(\boldsymbol{k})$ is given by (Batchelor 1953, equation 3.4.12)

$$\Phi_{ij}(\boldsymbol{k}) = \frac{E(k)}{4\pi k^2}\left(\delta_{ij} - \frac{k_i k_j}{k^2}\right), \tag{84}$$

where δ_{ij} is the Kronecker delta, $E(k)$ is the energy spectrum, and

$$\langle u^2 \rangle = \int \mathrm{d}^3\boldsymbol{k}\, \Phi_{ii}(\boldsymbol{k}). \tag{85}$$

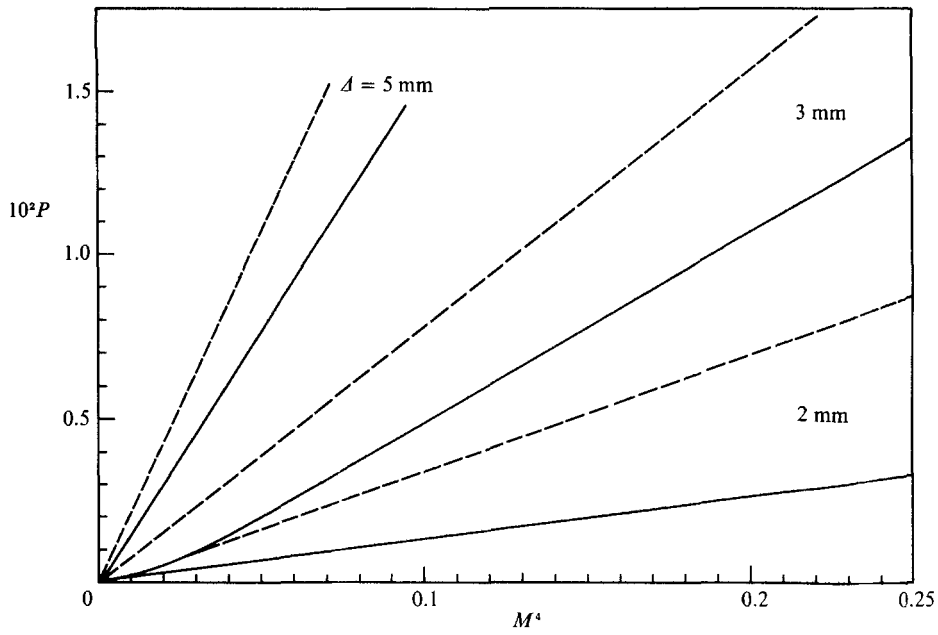

FIGURE 11. The quantity 10^2P, equation (71), versus M^4 for three values of the channel width $\Delta = 2, 3, 5$ mm. Solid lines, GISS; dashed lines, DIA.

The velocity covariance is a second-rank covariant tensor. Applying the coordinate change (84) to $\Phi_{ij}(\boldsymbol{k})$ yields

$$\Phi_{11}(\boldsymbol{k}') = N\left(\alpha(\boldsymbol{k}') + k_1' \frac{\partial \alpha}{\partial k_1'}\right)^2 \Phi_{11}(\boldsymbol{k}), \tag{86a}$$

$$\Phi_{22}(\boldsymbol{k}') = N\Phi_{22}(\boldsymbol{k}), \quad \Phi_{33}(\boldsymbol{k}') = N\Phi_{33}(\boldsymbol{k}), \tag{86b, c}$$

where a normalization coefficient N has been added to these expressions to ensure that the mean kinetic energy is identical to that of the original flow. The new correlation tensor now describes a flow for which all lengths are elongated by a factor α in the x_1 direction.

To calculate N, note that the kinetic energy (per unit mass) in the new coordinate system is

$$\frac{1}{2}\int \Phi_{ii}(\boldsymbol{k}')\,\mathrm{d}^3\boldsymbol{k}' = \tfrac{1}{2}N\int [h_1^2\Phi_{11}(\boldsymbol{k}) + \Phi_{22}(\boldsymbol{k}) + \Phi_{33}(\boldsymbol{k})]\frac{\mathrm{d}^3\boldsymbol{k}}{h_1 h_2 h_3}, \tag{87}$$

where $$h_1 = \alpha + k_1' \frac{\partial \alpha}{\partial k_1'}, \quad h_2^2 = 1 + k_1'^2\left(\frac{\partial \alpha}{\partial k_2'}\right)^2, \quad h_3^2 = 1 + k_1'^2\left(\frac{\partial \alpha}{\partial k_3'}\right)^2.$$

To ensure that the mean kinetic energy is identical to the original flow, (87) is equated to $\frac{1}{2}(R_{11}+R_{22}+R_{33}) = \frac{3}{2}R_0$ for isotropic R_{ii}, ($R_0 = R_{ii} \equiv \int \Phi_{ii}(\boldsymbol{k})\,\mathrm{d}^3\boldsymbol{k}$, no sum on the indices).

For the case of α = constant, the resulting equation is solved for N and we find that

$$N = \frac{3\alpha}{\alpha^2+2}, \quad \alpha \text{ constant}. \tag{88}$$

There is a second choice that can be made for the function α for which the normalization coefficient N can be easily computed, i.e.

$$\alpha(\boldsymbol{k}') = 1 + k_0/k_1', \tag{89}$$

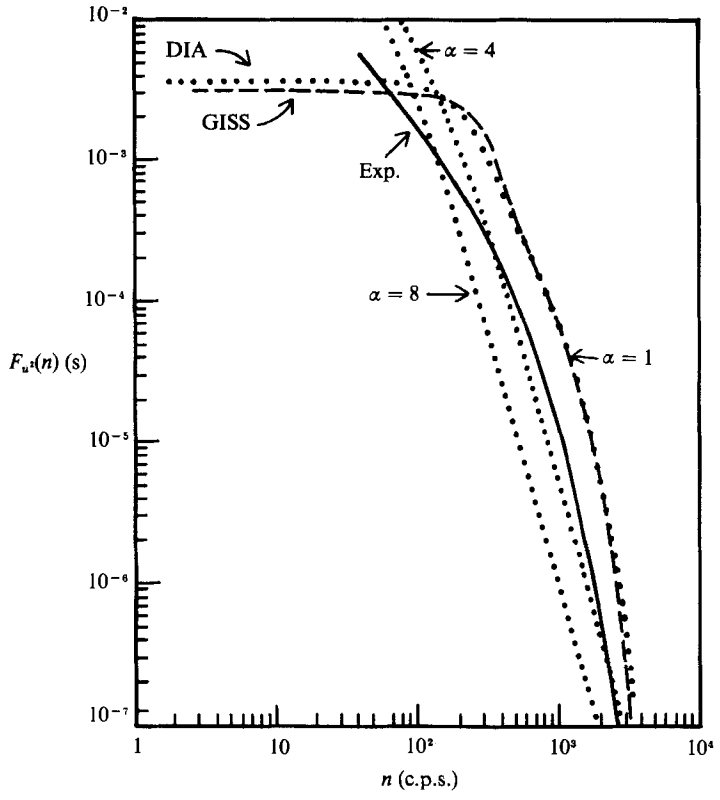

FIGURE 12. Same as figure 8, but also for $\alpha = 4$ and 8.

where k_0 is a constant. (In practice, to avoid the divergence at the origin a cutoff wavenumber was introduced in this function below which α was taken to be constant.) With this choice of α, $h_1 = h_2 = h_3 = 1$ and we find that $N = 1$.

11.1. *One-dimensional spectra*

The one-dimensional energy spectrum in the physical coordinate system is given by

$$E_1(k_1') = 2\int \mathrm{d}^2\boldsymbol{\kappa}' \Phi_{11}(\boldsymbol{k}'), \tag{90}$$

where $\kappa'^2 = k_2'^2 + k_3'^2 = \kappa^2$. After changing the variable of integration to

$$k^2 = k_1^2 + \kappa^2 = \alpha^2 k_1' + \kappa^2,$$

the one dimensional energy spectrum in the physical variables is

$$E_1(k_1') = N\int_{\alpha k_1'}^{\infty} h_1^2 \frac{E(k)}{k}\left(1 - \frac{\alpha^2 k_1'^2}{k^2}\right)\mathrm{d}k. \tag{91}$$

Figure 12 is a plot of the observed $E_1(k_1')$ for $R_{\mathrm{exp}} = 30800$ (actually, we plot $F_{\tilde{u}^2}(n)$, see (35)) compared to that calculated using the DIA spectrum with constant α. The scale factor α is a free parameter and figure 12 displays the results for $\alpha = 1$, 4, and 8. This procedure has provided a qualitative improvement over the $\alpha = 1$ result. The turnover of the spectrum, originally occurring at $n \sim 200\ \mathrm{s}^{-1}$, has moved to

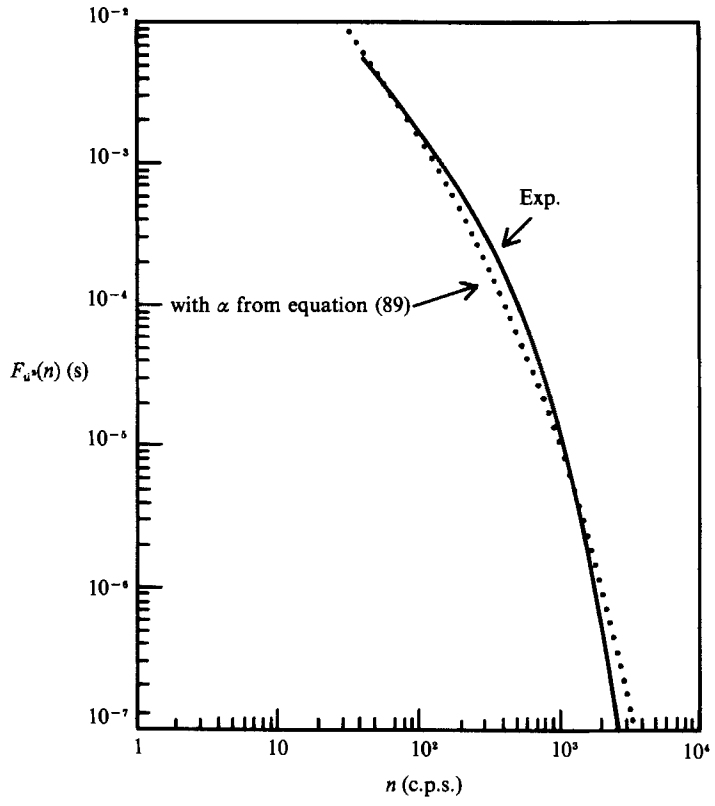

FIGURE 13. Same as figure 8, but for $\alpha = \alpha_0$ for $k_1' D \leqslant 1$, and $\alpha = 1 + (\alpha_0 - 1)/k_1' D$ for $k_1' D > 1$, with $\alpha_0 = 5$. This result was calculated using the DIA turbulence spectrum.

frequencies (i.e. wavenumbers) beyond the lowest observed, in concert with the observations.

Figure 13 is a plot comparing the experimental data for the one-dimensional spectrum and a calculation with α given by (89). We have chosen the cutoff wavenumber to be $k_1' D = 1$, below which we take $\alpha = \alpha_0 = 5$. The constant k_0 is chosen to make α continuous through this cutoff, i.e. $k_0 = (\alpha_0 - 1)/D$. Obviously, the inclusion of anisotropy in this way such that the elongation of the eddies decreases for the smaller scale sizes has greatly improved our fit to the data. Note that the value of α_0 which provides such a close fit to the data is in the range indicated by the constant-α results.

Naturally, it is not to be expected that the procedure presented here would provide a perfect fit to the data. However, the results do suggest that accounting for anisotropy considerably improves the fitting of the one-dimensional spectra. It is also to be noted that there is no unique choice for the anisotropy function α. We have used the simplest choice, constant α, and a second more physical choice for which the stretching of scales in the downstream direction decreases with decreasing scale size. With increased complexity of the modelling of the effects of anisotropy, we have seen our fit to the data improve markedly. The calculations of the effect of anisotropy on the pressure fluctuations and scattering of a monochromatic beam presented below were done using a constant α.

11.2. *Pressure fluctuations*

For the anisotropic case with constant α, the calculation of the pressure fluctuations is similar to that done in §9. For the amplitude of the pressure fluctuations, we write

$$\frac{\langle p^2(x_2)\rangle}{\rho^2} = \int \mathrm{d}^3\boldsymbol{k}'\,\Pi(\boldsymbol{k}', x_2'), \tag{92}$$

$$\Pi(\boldsymbol{k}', x_2') = 4s_0^2 \frac{2\pi}{\Delta} \sum_{n=-\infty}^{\infty} \delta(k_2' - k_2^{(n)}) \frac{k_1^2}{\kappa'^2}\frac{k_2^2}{k'^4} \Phi_{22}(\boldsymbol{k}')\,(\Gamma_1^2(\boldsymbol{k}', x_2') + \Gamma_2^2(\boldsymbol{k}', x_2')), \tag{93}$$

$$\Gamma_1(\boldsymbol{k}', x_2') = \frac{\cosh\kappa'(\frac{1}{2}\Delta - x_2)}{\sinh\frac{1}{2}\kappa'\Delta} + \frac{\kappa'}{k_2'}\left(1 - 2\frac{x_2}{\Delta}\right)\sin k_2' x_2' - \frac{4\kappa'}{k'^2\Delta}\cos k_2' x_2', \tag{94}$$

$$\Gamma_2(\boldsymbol{k}', x_2') = \frac{2}{k_2'\Delta}\left(1 - 2\frac{\kappa'^2}{k'^2}\right)\frac{\sinh\kappa'(\frac{1}{2}\Delta - x_2)}{\cosh\frac{1}{2}\kappa'\Delta} + \frac{\kappa'}{k_2'}\left(1 - 2\frac{x_2}{\Delta}\right)\cos k_2' x_2' + \frac{4\kappa'}{k'^2\Delta}\sin k_2' x_2', \tag{95}$$

with $\delta(x)$ the Dirac delta function, $k_2^{(n)} = 2\pi n/\Delta$, and $\kappa'^2 = k_1'^2 + k_3'^2$. In (92)–(95), the integration variables and position variable have been written as $\boldsymbol{k}'$, and x_2', respectively, in order to emphasize that these are the physical coordinates, i.e. those stretched in the streamwise direction. Although we only know $E(k)$ in terms of wavenumbers from which the stretching has been removed, we do know how to relate $\Phi_{ij}(\boldsymbol{k}')$ to $\Phi_{ij}(\boldsymbol{k})$. Now change variables in the integral from $\boldsymbol{k}'$ to $\boldsymbol{k}$. Working in the coordinate system defined by

$$k_1 = k\sin\theta\cos\phi, \quad k_2 = k\cos\theta, \quad k_3 = k\sin\theta\sin\phi,$$

the quantities κ'^2 and k'^2 are given by

$$\kappa'^2 = k^2\sin^2\theta\left(1 - \frac{\alpha^2 - 1}{\alpha^2}\cos^2\phi\right) \equiv k^2 f(\phi)\sin^2\theta, \tag{96}$$

$$k'^2 = k^2\left(1 - \frac{\alpha^2 - 1}{\alpha^2}\sin^2\theta\cos^2\phi\right) \equiv k^2 g(\theta, \phi). \tag{97}$$

Using $\mathrm{d}^3\boldsymbol{k}' = \mathrm{d}^3\boldsymbol{k}/\alpha$, we have from (92)

$$\frac{\langle p^2(x_2;\alpha)\rangle}{\rho^2} = \frac{1}{\alpha}\int \mathrm{d}^3\boldsymbol{k}\,\Pi(\boldsymbol{k}, x_2;\alpha), \tag{98}$$

where

$$\Pi(\boldsymbol{k}, x_2;\alpha) = \frac{s_0^2}{\pi^2}\frac{N}{\alpha^2}\frac{2\pi}{\Delta}\sum_{n=-\infty}^{\infty}\delta(k_2 - k_2^{(n)})\frac{E(k)}{k^4}\frac{\sin^2\theta\cos^2\phi}{f(\phi)\,g^2(\theta,\phi)}\frac{k_2^2}{k^2}(\Gamma_1^2(\boldsymbol{k}', x_2) + \Gamma_2^2(\boldsymbol{k}', x_2)), \tag{99}$$

and Γ_1 and Γ_2 are given by (94) and (95). Since the integrand is symmetric in the summation index n and the $n = 0$ term vanishes, we find for the amplitude of the pressure fluctuations

$$\frac{\langle p^2(x_2;\alpha)\rangle}{\rho^2} = \frac{4N}{\alpha^3}\frac{s_0^2}{\Delta}\int_0^{2\pi}\mathrm{d}\phi\int_{2\pi/\Delta}^{\infty}\mathrm{d}k\,\frac{E(k)}{k^3}\frac{\cos^2\phi}{f(\phi)}\sum_{n=1}^{[k\Delta/2\pi]}\left(\frac{2\pi n}{k\Delta}\right)^2 \times\left[1 - \left(\frac{2\pi n}{k\Delta}\right)^2\right]\frac{1}{g(\theta_n,\phi)}[\Gamma_1^2(\boldsymbol{k}', x_2) + \Gamma_2^2(\boldsymbol{k}', x_2)], \tag{100}$$

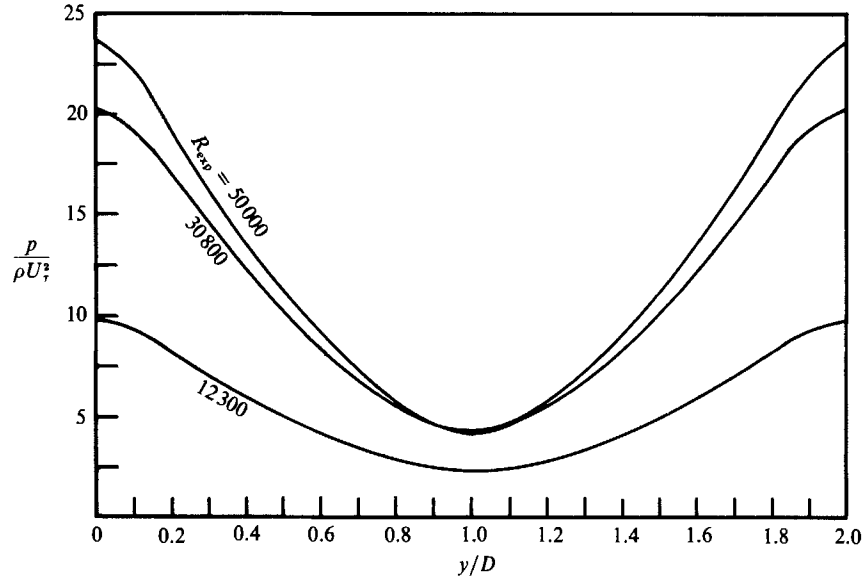

FIGURE 14. Same as figure 10, but for $\alpha = 4$.

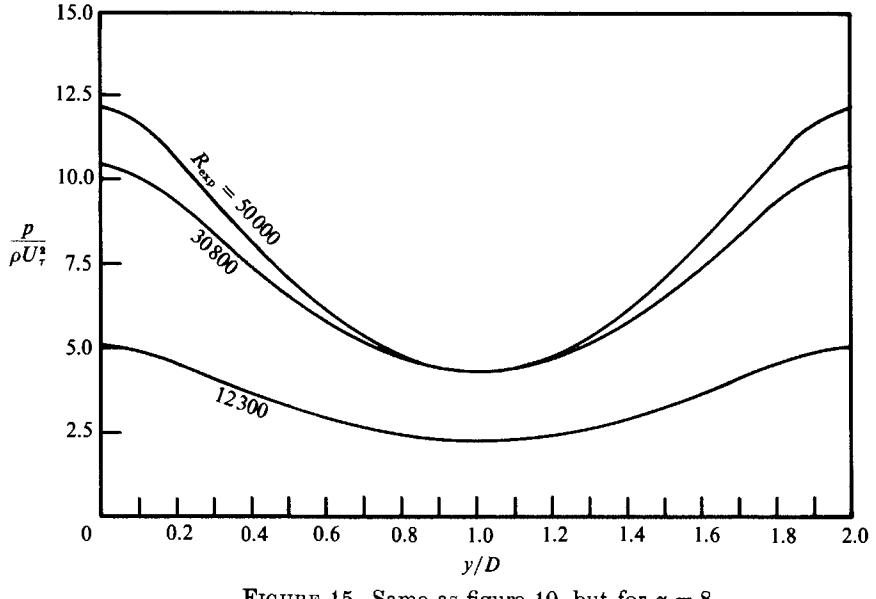

FIGURE 15. Same as figure 10, but for $\alpha = 8$.

where

$$\sin^2\theta_n = 1 - \left(\frac{2\pi n}{k\Delta}\right)^2. \tag{101}$$

Equation (100) was integrated numerically using the DIA spectrum for $\alpha = 4, 8$, and the results for Reynolds numbers of 12300, 30800, and 50000 are displayed in figures 14 and 15. Relative to the $\alpha = 1$ case, the pressure at the wall is reduced by a factor of approximately $1/\alpha$, i.e. with the pressure in units of ρU_τ^2,

$$p_{\text{wall}}(\alpha) \approx \frac{1}{\alpha} p_{\text{wall}}(\alpha = 1). \tag{102}$$

			10^2P		
R_{exp}	M	M_b	$\alpha = 1$	$\alpha = 4$	$\alpha = 8$
			$\Delta = 2$ mm		
12300	0.286	0.252	8.48×10^{-3}	2.80×10^{-3}	7.86×10^{-4}
30800	0.715	0.638	0.920	0.315	8.89×10^{-2}
50000	1.16	1.04	5.99	2.25	0.662
			$\Delta = 3$ mm		
12300	0.190	0.168	3.77×10^{-3}	1.24×10^{-3}	3.49×10^{-4}
30800	0.477	0.425	0.410	0.140	3.95×10^{-2}
50000	0.774	0.694	2.71	1.01	0.295
			$\Delta = 5$ mm		
12300	0.114	0.101	1.36×10^{-3}	4.47×10^{-4}	1.26×10^{-4}
30800	0.286	0.255	0.148	5.05×10^{-2}	1.42×10^{-2}
50000	0.465	0.416	0.987	0.363	0.106

TABLE 6. Values of 10^2P for full channel width $\Delta = 2$, 3, and 5 mm

The pressures at midchannel have undergone relatively small changes relative to the isotropic ($\alpha = 1$) calculation, i.e.

$$p_{\text{midch}}(\alpha) \approx p_{\text{midch}}(\alpha = 1). \tag{103}$$

It seems clear that the inclusion of the effects of anisotropy in the calculation of the amplitude of the pressure fluctuations has greatly improved our predictions of the wall pressures.

11.3. *Fraction of scattered power, P*

We have also applied the above procedure to the modelling of the effects of anisotropy on the attenuation of a laser beam propagating through a turbulent channel flow. With the fraction of scattered power defined by (72) and (73), we integrated (73) over the physical variables, using the DIA spectrum and the expressions from above for the anisotropic pressure function. The scattered fraction P was calculated for channel widths $\Delta = 2$, 3, and 5 mm at a variety of Mach numbers and the results are presented in table 6 and displayed in figure 16 along with the experimental results of Albrecht & Sutton (1987) at these values of Δ. The errors on the experimental results are roughly $\pm 35\%$. The Mach number M_b used in figure 16 is the Mach number based on the bulk velocity, U_m. Using (14*a*) and (15*b*), we find that M_b is related to the Mach number M (based on the midchannel velocity U_0) by

$$M_b = M\left[1 - \frac{2.53}{9.268 R_{exp}^{0.089}}\right]. \tag{104}$$

It was found that the model fitted the data very well with $\alpha = 6$ for $\Delta = 2$ mm, $\alpha = 4$ for $\Delta = 3$ mm, and $\alpha = 5$ for $\Delta = 5$ mm. These are the best-fit results; however, within the errors, the data can be adequately fitted for $\alpha = 5$. It was found that over the range $1 \leqslant \alpha \leqslant 10$, the scattered fraction P decreases with α roughly as

$$P(\alpha) \approx P(\alpha = 1)\, e^{-(\alpha-1)/3}. \tag{105}$$

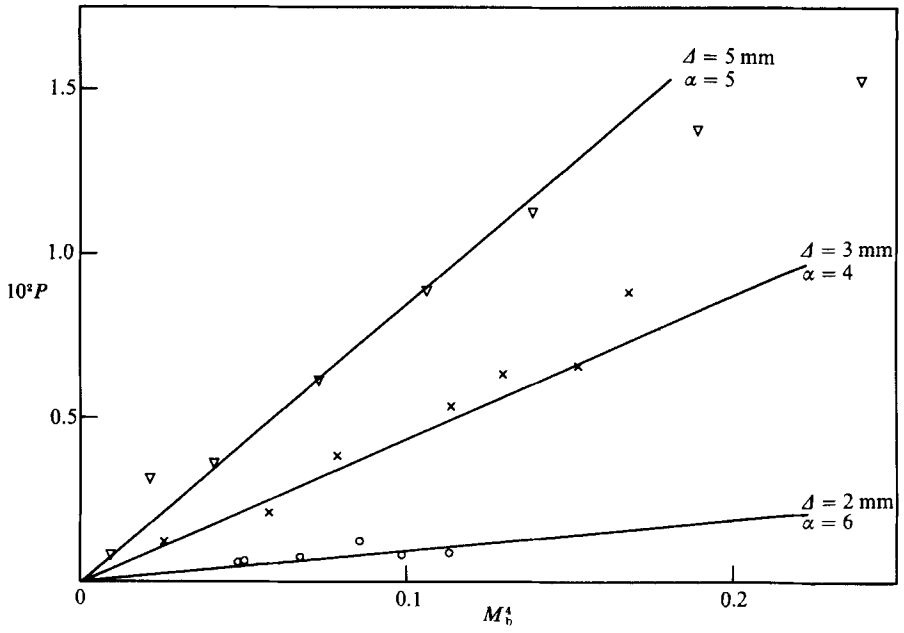

FIGURE 16. The quantity 10^2P versus the fourth power of the bulk Mach number, M_b^4 (see text), for three values of channel width $\Delta = 2$, 3, and 5 mm. The best-fit value of α is shown. The experimental data (from Albrecht & Sutton 1987) are represented as ∇ for the 5 mm results, $\times$ for the 3 mm results, and $\bigcirc$ for the 2 mm results.

12. Parameterization of the results

The scattered fraction P for an isotropic system ($\alpha = 1$) is given by

$$P(\alpha = 1) = 1 - \exp(-\sigma_\phi^2). \tag{106}$$

As we have seen, the dependence on the general anisotropy parameter α can be represented by

$$P(\alpha) = P(\alpha = 1)\, e^{-(\alpha-1)/3}. \tag{107}$$

We have managed to write σ_ϕ^2 as

$$\sigma_\phi^2 = C_0 D^{3.644} M^{5.644} \gamma^{2.822} \mu^{-2} p^{0.822} \rho^{1.178} \nu^{-1.644} g(R_{\exp}) \tag{108}$$

or, equivalently,

$$\sigma_\phi^2 = C_1 D^2 M^4 \frac{\gamma^2 \rho^2}{\mu^2} f(R_{\exp}), \tag{109}$$

where D is the channel half-width in mm, M is the Mach number based on the midchannel velocity U_0 (see (104) for the conversion to M_b, the Mach number based on the bulk velocity), γ is the ratio of specific heats, μ is the atomic weight, p is the pressure in atmospheres, ρ is the density in g cm^{-3}, ν is the viscosity in cm^2 s^{-1}, $R_{\exp} = U_0 D/\nu$ with U_0 the velocity of the flow at midchannel, $C_0 = 7.6288 \times 10^2$, and $C_1 = 0.38883$. The functions $g(R_{\exp})$ and $f(R_{\exp})$ are given by

$$g(R_{\exp}) = \sum_{n=0}^{5} a_n R_{\exp}^n, \tag{110}$$

$$f(R_{\exp}) = R_{\exp}^{1.644} g(R_{\exp}), \tag{111}$$

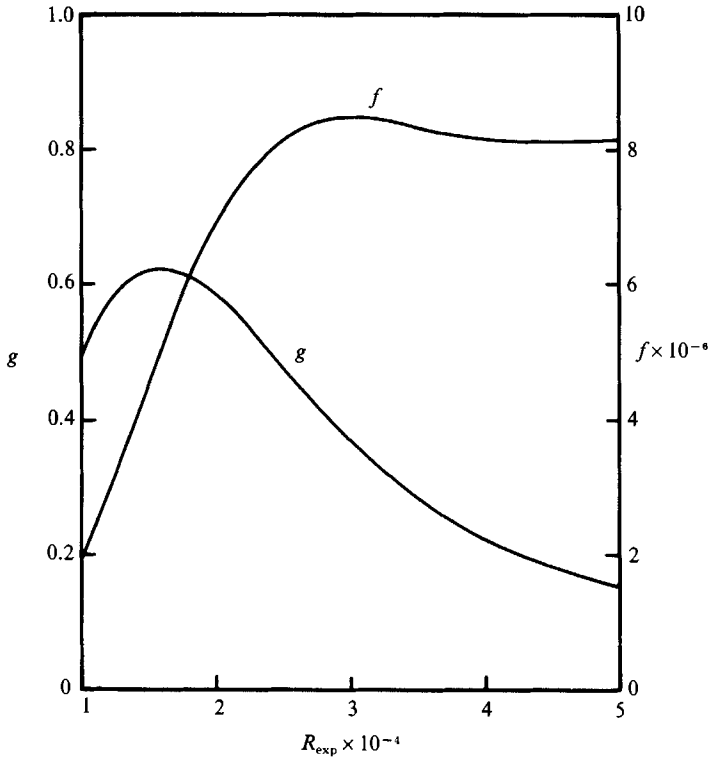

FIGURE 17. The functions f and g used for the parameterization of the scattered fraction P are plotted here for $10^4 \leqslant R_{exp} \leqslant 5 \times 10^4$. Note that for $R_{exp} \geqslant 2.5 \times 10^4$, f is approximately constant, thus P will increase as M^4 for constant Δ.

with
$$a_0 = -1.0, \quad a_1 = 2.7798 \times 10^{-4}, \quad a_2 = -1.6914 \times 10^{-8},$$
$$a_3 = 4.5123 \times 10^{-13}, \quad a_4 = -5.6832 \times 10^{-18}, \quad a_5 = 2.7697 \times 10^{-23}. \tag{112}$$

Figure 17 is a plot of the functions $f(R_{exp})$ and $g(R_{exp})$ for $10^4 \leqslant R_{exp} \leqslant 5 \times 10^4$. Note that in the range $2.5 \times 10^4 \leqslant R_{exp} \leqslant 5 \times 10^4$, the function $f(R_{exp})$ is approximately constant. The lower end of this range, i.e. $R_{exp} = 2.5 \times 10^4$, corresponds to $M_b^4 = 7.11 \times 10^{-2}$ (2 mm/Δ)^4 for the gas parameters used here and Δ = full channel width. Thus for M_b^4 greater than this, the quantity σ_ϕ^2 will increase with Mach number as M^4 for constant D and increase as D^2 for constant M. Experimentally, it has been found at constant M, P increases as D^a with $a = 1.75 \pm 0.25$. Equations (106)–(112) reproduce the theoretical results to better than 5%.

13. Summary and conclusions

By inspecting our results, it can be concluded that the GISS model and the DIA provide a reasonable first description of both turbulent bulk properties and properties that depend strongly on the large-eddy part of the energy spectrum. Several reservations have to be discussed and directions for future work pointed out.

First, the DIA yields larger values for the wall pressure and fraction of scattered power than the GISS model. This behaviour can be understood by inspecting, for example, (65) which shows that the largest contribution to $\Pi(\boldsymbol{k})$, and ultimately to P, comes from the small-k region of the turbulent energy spectrum. As one can see

from figure 4, at low wavenumbers the GISS $E(k)$ is 'skinnier' than the one derived from DIA. This means that the contribution to $\Pi(k)$ from the GISS model begins only at, say, $kD = 15$, while in the DIA case the contribution begins earlier, i.e. at smaller wavenumbers. (The DIA energy spectrum extends in principle to zero wavenumber, but the integration over the angles in (64) and the presence of the delta function in (65) force the first contribution to begin at $kD = \pi$.) The physical reason behind the different low-k behaviour of the two spectral functions is known. The DIA includes backscatter, i.e. energy transferred from the high-k region into the low-k region. By contrast, the present version of the GISS model is a cascade model with no backscatter as yet. While this limitation had been recognized in the earlier work of Canuto *et al.* (1987) and Hartke *et al.* (1988), it had never been evidenced as clearly as in the present case, since our earlier works were primarily concerned with the description of turbulent bulk properties which are relatively insensitive to the small-k behaviour of the turbulent spectral function. Work to include backscatter in the GISS model is now in progress.

A second comment concerns the role of shear and the way it has been treated in the present paper. The work of Tchen (1953) has demonstrated that the shear may play two roles; as a source of energy and as a force interacting with the eddies. While the first role is always present, the second becomes important only when the shear s is of the same order or larger than the eddy vorticity in a given wavenumber region. When this is the case, a resonance takes place which may be more important than the effects of nonlinear transfer among the eddies, represented by the function $T(k)$ in (1). When this type of resonance dominates over the other forces, Tchen's model predicts the existence of a k^{-1} region in the energy spectrum, which has indeed been observed. Our model does not include this resonance effect, the shear playing in fact only one role, that of a source of energy drained from the mean flow. This can clearly be seen by inspecting (1) and (2) where the presence of shear is confined entirely to the left-hand side of the equation in the rate $n_s(k)$, whose form is given by (24). It is clearly seen that of the two terms, the first, Im (Q), is proportional to the shear, $U'(y)$, while the other term represents a sink due to viscosity.

A third comment refers to the choice of the growth rate. Orszag & Patera (1983) (hereinafter referred to as O–P) have pointed out that the adoption of a Poiseuille flow with a central line velocity U_0 (used to construct a Reynolds number which is then identified with the experimental value), leads to a growth rate that, being viscid in nature is naturally rather slow. In fact, the fastest instability occurs at around $R = 48000$ and its maximum value (n_s/n_*) is only 0.0076. O–P discovered that there is a secondary, three-dimensional instability that grows much faster than the original instability. The O–P discovery is an important one in many respects, but particularly when one is concerned with the problem of the transition between laminarity and turbulence, since it explains in a natural way (i.e. without free parameters) experimentally important features that would otherwise be left unexplained (see Stuart 1981), the most important being the well known fact that linear analysis predicts a breakdown of laminarity at $R_{exp} = 5772$ while the experimental value is close to $R_{exp} \sim 2500$. It is much less clear, however, whether the O–P secondary instability and its corresponding growth rate is directly relevant to our problem, where we have to deal with one important aspect that does not enter into the O–P problem, namely the fact alluded to previously, that in the construction of n_s for our problem we must somehow take into account the renormalizing effect of the presence of turbulence itself. The physical model that we have proposed in §4 can be viewed as a way to renormalize the central line velocity due to the presence of turbulence.

Another important aspect of the physical effect brought about by the existence of the O–P secondary waves is displayed in figure 4 of O–P, where it is shown that the growth rate versus Reynolds number curve reaches a maximum and then saturates rather than decreasing as it would in the case of a viscid instability. Two facts must be noticed. The maximum value of the O–P growth rate is around 0.1, which is the same as we have obtained using our renormalization (see figure 3). Secondly, as it is also clear from figure 2, in the region of Reynolds numbers of interest in this problem, the growth rates have similar maximum values, thus indicating that we are dealing with a region where the stabilizing effect of decreasing viscosity has not yet taken place. The numerical similarity between our results and those of O–P constitutes, however, no guarantee that the O–P mechanism (to generate a growth rate) and our method are physically equivalent. Since our results for the bulk properties are in general smaller than the experimental values, it is conceivable that the use of an O–P growth rate together with a renormalization of some of the physical parameters could yield better results. Since, however, the solution of the O–P equation, which in turn requires the exact solution of the Navier–Stokes equations for the two-dimensional flow field, would be a non-trivial addition to our problem, we decided in this first paper to adopt the physical argument discussed above. The use of the O–P growth rate mechanism is presently under investigation.

In conclusion, while the use of theoretical models of turbulence has reproduced several properties of turbulent channel flow, limitations have also appeared. Work to include backscatter in the GISS model and to understand the role of the secondary instability is now in progress.

The authors would like to thank H. Robey and S. Sutton for many helpful discussions and D. Henningson for providing the use of his Orr–Sommerfeld code.

REFERENCES

ALBRECHT, G. F. & SUTTON, S. 1987 *LLNL Rep.*, October 1987.

BATCHELOR, G. K. 1951 *Proc. Camb. Phil. Soc.* **47**, 359.

BATCHELOR, G. K. 1953 *The Theory of Homogeneous Turbulence.* Cambridge University Press.

BLAKE, W. K. 1970 *J. Fluid Mech.* **44**, 637.

CANUTO, V. M., GOLDMAN, I. & CHASNOV, J. 1987 *Phys. Fluids* **30**, 3391.

CLARK, J. A. 1968 *Trans. ASME* D: *J. Basic Engng* **90**, 455.

COMTE-BELLOT, G. 1963 Ecoulement turbulent entre deux parois parallelles. Ph.D. thesis, University of Grenoble, France.

DRAZIN, P. G. & REID, W. H. 1982 *Hydrodynamic Stability.* Cambridge University Press.

HANDLER, R. A., HANSEN, R. J., SAKELL, L., ORSZAG, S. A. & BULLISTER, E. 1984 *Phys. Fluids* **27**, 579.

HANJALIC, K. & LAUNDER, B. E. 1972 *J. Fluid Mech.* **52**, 609.

HARTKE, G. J., CANUTO, V. M. & DANNEVIK, W. P. 1988 *Phys. Fluids* **31**, 256.

HINZE, J. O. 1975 *Turbulence.* McGraw-Hill.

HOGGE, C. B., BUTTS, R. R. & BURLAKOFF, M. 1974 *Appl. Opt.* **13**, 1065.

HUSSAIN, A. K. M. F. & REYNOLDS, W. C. 1975 *Trans. ASME* I: *J. Fluids Engng* **97**, 568.

IERLEY, G. R. & MALKUS, W. V. R. 1988 *J. Fluid Mech.* **187**, 435.

JOHANSSON, A. V. & ALFREDSSON, P. H. 1982 *J. Fluid Mech.* **122**, 295.

KIM, J., MOIN, P. & MOSER, R. 1987 *J. Fluid Mech.* **177**, 133.

KRAICHNAN, R. H. 1956*a* *J. Acoust. Soc. Am.* **28**, 64.

KRAICHNAN, R. H. 1956*b* *J. Acoust. Soc. Am.* **28**, 378.

KRAICHNAN, R. H. 1964*a* *Phys. Fluids* **7**, 1030.
KRAICHNAN, R. H. 1964*b* *Phys. Fluids* **7**, 1048.
LAUFER, J. 1951 *Nat. Adv. Commn. Aeron., Rep.* 1053.
LESIEUR, M. 1987 *Turbulence in Fluids*. M. Nijhoff.
LESLIE, D. C. 1973 *Developments in the Theory of Turbulence*. Clarendon.
LIN, C. C. 1955 *The Theory of Hydrodynamic Stability*. Cambridge University Press.
MARTIN, P. C., SIGGIA, E. D. & ROSE, H. A. 1973 *Phys. Rev.* A **8**, 423.
MOIN, P. & KIM, J. 1982 *J. Fluid Mech.* **118**, 341.
MONIN, A. S. & YAGLOM, A. M. 1975 *Statistical Fluid Mechanics* (M.I.T. Press).
OBSZAG, S. A. & PATERA, A. T. 1983 *J. Fluid Mech.* **128**, 347.
REYNOLDS, W. C. & TIEDERMAN, W. G. 1967 *J. Fluid Mech.* **27**, 253.
STUART, J. T. 1981 In *Transition and Turbulence* (ed. R. E. Meyer), p. 77. Academic.
SYNGE, J. L. 1938 *Semi-Centenn. Publ. Am. Math. Soc.* **2**, 227.
TATARSKII, V. I. 1961 *Wave Propagation in a Turbulent Medium*. McGraw-Hill.
TCHEN, C. M. 1953 *J. Res. Natl Bur. Stand.* **50**, 51.
TOWNSEND, A. A. 1976 *The Structure of Turbulent Shear Flow*. Cambridge University Press.
WILLMARTH, W. W. 1975 *Ann. Rev. Fluid Mech.* **7**, 13.